Available online at www.sciencedirect.com

ScienceDirect

Geochimica et Cosmochimica Acta 303 (2021) 92–109

Geochimica et Cosmochimica Acta

www.elsevier.com/locate/gca

B isotopic constraints on the role of H_2O in mantle wedge melting

Yang Yu [a,b,c], Xiao-Long Huang [a,b,c,*], Min Sun [d], Jin-Long Ma [a,b,c]

[a] State Key Laboratory of Isotope Geochemistry, Guangzhou Institute of Geochemistry, Chinese Academy of Sciences, Guangzhou 510640, China
[b] CAS Center for Excellence in Deep Earth Science, Guangzhou 510640, China
[c] Southern Marine Science and Engineering Guangdong Laboratory (Guangzhou), Guangzhou 511458, China
[d] Department of Earth Sciences, The University of Hong Kong, Pokfulam Road, Hong Kong

Received 10 January 2021; accepted in revised form 31 March 2021; available online 20 April 2021

Abstract

The role of water on melting in the mantle wedge is still debated due to large uncertainty on the estimates of H_2O flux beneath arcs. B has been proven as an effective proxy for water flux because B and H_2O show similar chemical behaviors during subduction. The Habahe mafic dikes from the Chinese Altai were emplaced within a narrow area (<20 km from south to north) during the northward subduction of the Junggar Ocean in the middle Paleozoic. These dikes have been classified into four types with distinct geochemical and Sr-Nd-Hf-Pb isotopic compositions, which originated from mantle sources metasomatized by different subduction components, including melts from subducted sediments (Type-I, Type-IV), fluids from subducted sediments (Type-II), and melts from subducted oceanic crust (Type-III). We present B content and isotope data for the Habahe mafic dikes to investigate the influence of subduction components on melting in the mantle wedge. Type-I and -III mafic dikes all have negative $\delta^{11}B$ values (−7.7‰ to −5.0‰) with variable B contents (3.65–13.4 ppm) and B/Nb ratios (2.10–7.39), indicating B isotopically light features for the subducted sediments and oceanic crust. Type-II mafic dikes have lower B contents (3.97–9.90 ppm) and higher B/Nb ratios (7.07–14.4) than Type-I mafic dikes, with a wide range of $\delta^{11}B$ values from −7.8‰ to −2.7‰. This suggests that their mantle source may have been metasomatized by fluids from subducted serpentinite besides fluids from subducted sediments. Type-IV mafic dikes have higher B contents (17.0–27.5 ppm) and B/Nb ratios (25.0–40.8), and heavier B isotopic compositions ($\delta^{11}B = -2.9‰$ to +3.5‰) than Type-I mafic dikes. This indicates involvement of fluids from the slab serpentinite in metasomatism of their mantle source in addition to melts from the subducted sediments. The Habahe mafic dikes show wide range of B/Nb ratios, suggesting that different amounts of water were added into their mantle sources. These dikes exhibit variable Zr/Yb and Nb/Yb ratios, and constantly low TiO_2/Yb, indicating their formation through different degrees melting of depleted mantle sources. Their Zr/Yb and Nb/Yb ratios are negatively correlated with B/Nb, which reflects elevation of the melting degree of their mantle sources as increasing water input. Similar trends are also observed in basalts from global arcs and their major and trace elements correlate well with B/Nb ratios. Thus, water flux should play an important role on melting in the mantle wedge and control magma compositions of the arcs.

Keywords: Central Asian Orogenic Belt; Chinese Altai; Arc magmatism; B isotope; Water; Mantle wedge

1. INTRODUCTION

The subducted slab, including sediments, altered oceanic crust and serpentinite, can sink into the deep mantle and release water into the mantle wedge via aqueous fluids and hydrous melts (Elliott et al., 1997; Kessel et al., 2005; Spandler and Pirard, 2013). Addition of H_2O-rich

* Corresponding author at: State Key Laboratory of Isotope Geochemistry, Guangzhou Institute of Geochemistry, Chinese Academy of Sciences, Guangzhou 510640, China.
E-mail address: xlhuang@gig.ac.cn (X.-L. Huang).

https://doi.org/10.1016/j.gca.2021.03.032
0016-7037/

components will promote melting of the mantle wedge because water can dramatically lower the peridotite solidus (Mysen and Boettcher, 1975; Kawamoto and Holloway, 1997; Grove et al., 2002; Till et al., 2012; Green, 2015). Emplacement of arc magmas will transfer juvenile materials from the mantle to the crust, responsible for continental growth (Mysen and Boettcher 1975; Grove et al., 2012). Understanding the role of water on melting in the mantle wedge is thus an essential step towards understanding the geochemical recycling processes between mantle and crust (Sisson and Grove, 1993; Carmichael, 2002; Pichavant and MacDonald, 2007).

Both experimental and modelling results suggest that increasing amount of water will elevate the melting extent of mantle peridotite (Gaetani and Grove, 1998; Kelley et al., 2010; Till et al., 2012; Green, 2015). In this sense, the mantle wedge in global subduction zones may undergo different extents of melting processes due to large variations of H_2O flux beneath arcs (van Keken et al., 2011). However, the estimates of H_2O flux in global subduction zones show poor correlations with island arc basalt (IAB) compositions (Fig. A1), which has caused hot debates on the role of H_2O in the mantle wedge melting processes (Turner and Langmuir, 2015a, b; Turner et al., 2016). Some studies exclude the role of H_2O on melting in the mantle wedge, and consider other factors such as the physical state of subducting plate-mantle wedge (e.g., Grove et al., 2009; Wada and Wang, 2009), the thermal structure of mantle wedge (England and Katz, 2010; Perrin et al., 2018), or the age and thickness of overlying plate (Turner and Langmuir, 2015a, b; Turner et al., 2016). Indeed, these factors will influence the pressure and temperature of melting processes in the mantle wedge. It is also noteworthy that there are great uncertainties in estimating water flux beneath the arcs because many important factors in model calculations, such as slab age, slab dip, subduction velocity, initial input of water content and the lithology of the slab, are still poorly constrained (Rüpke et al., 2004; van Keken et al., 2011). Therefore, inaccurate estimates of water flux beneath the arcs may have caused misunderstanding for the role of H_2O on melting in the mantle wedge.

Boron is a strongly fluid mobile element and shows chemical behaviors similar to H_2O, with high incompatibility during dehydration and melting of the subducted slab (Leeman, 1996; Marschall et al., 2007; Ryan and Chauvel, 2014; De Hoog and Savov, 2018). Ratios of B to fluid-immobile trace elements, such as B/Nb and B/Zr, in IAB have been recently proven as an effective proxy for water flux during subduction (Manea et al., 2014; Konrad-Schmolke et al., 2016; Leeman et al., 2017; Cooper et al., 2020). This makes B a potential geochemical indicator to investigate the role of water in controlling melting of the mantle wedge. In addition, the mantle wedge is commonly characterized by low B content and light B isotopic compositions (e.g., $B = 0.077$ ppm; $\delta^{11}B = -7.1‰$; Marschall et al., 2017), while the subducting slab, including AOC, sediments and serpentinite, may have high B content and heavy B isotopic composition due to interaction with seawater ($B = \sim 4.4$ ppm; $\delta^{11}B = +39.61‰$; Foster et al., 2010) before entering the trench. Fluids and melts can effectively mobilize B from the subducted slab and will significantly change the B content and isotopic budget in the mantle wedge (Marschall et al., 2007; Wu and Stebbins, 2010; Kowalski and Wunder, 2018). Therefore, the B elemental and isotopic compositions of IAB can be used as a powerful indicator to explore influence of components from the subducted slab within a mantle wedge system.

The Chinese Altai, which is a key part of the southwestern Central Asian Orogenic Belt, underwent northward subduction of the Junngar Ocean, a segment of the Paleo-Asian Ocean, since the early Paleozoic (~470 Ma; Cai et al., 2011), and collided with the Junggar terrane during the late Paleozoic (~320 Ma; Fig. 1; Xiao et al., 2015). The subduction caused significant arc magmatism with voluminous emplacement of granitic plutons and mafic rocks (Yu et al., 2019). There were abrupt increase of juvenile materials in the crust and high temperature metamorphism in the Chinese Altai at around 400 Ma, which possibly record initiation of oceanic ridge subduction in this region (Sun et al., 2009; Jiang et al., 2010; Yu et al., 2017a, 2020). Mafic dikes were emplaced into the Habahe igneous complex in the south margin of the Chinese Altai at about 360 Ma, within a distance of <20 km from south to north (Fig. 1c; Yu et al., 2017a, 2020). The Habahe mafic dikes show variable Sr-Nd-Hf-Pb isotopic compositions, which have been interpreted as the metasomatism in their mantle sources by fluids and melts from the subducted sediments and/or melts from the subducted oceanic crust (Yu et al., 2017a, 2020). The different subduction components may have transferred variable amounts of water into their mantle sources and caused different melting processes of the mantle wedge. Thus, the Habahe mafic dikes possibly represent an example of varying degrees of melting of the mantle wedge due to input of different amount of water. In this study, we present B content and isotopic compositions for the Habahe mafic dikes. These data are combined with the previous Sr-Nd-Hf-Pb isotopes and trace element data to characterize the metasomatism of their mantle sources and demonstrate the influence of water flux on melting in the mantle wedge.

2. GEOLOGICAL BACKGROUND

The Chinese Altai is bounded by the Erqis Fault and separated from the Junggar terrane in the south (Fig. 1b) and is considered as an accretionary complex in the early Paleozoic without Precambrian basement (Xiao et al., 2015; Yu et al., 2017b). The details of tectonic units in the Chinese Altai had been described in previous publications (e.g., Windley et al., 2007; Sun et al., 2008; Yu et al., 2019). The Habahe igneous complex is exposed northeast of Habahe town with an area of ~450 km^2 (Fig. 1c), and intruded into Devonian strata which underwent low grade green schist metamorphism. The Habahe complex consists of biotite granite (381 ± 4 Ma to 359 ± 4 Ma), tonalite (371 ± 3 Ma) and mafic rocks, including gabbro (369 ± 3 Ma) and mafic dikes (~360 Ma) (Yu et al., 2017a, 2019, 2020). These rocks are massive and fresh without significant deformation and metamorphism (Yu et al., 2019). The Habahe mafic dikes vertically intruded

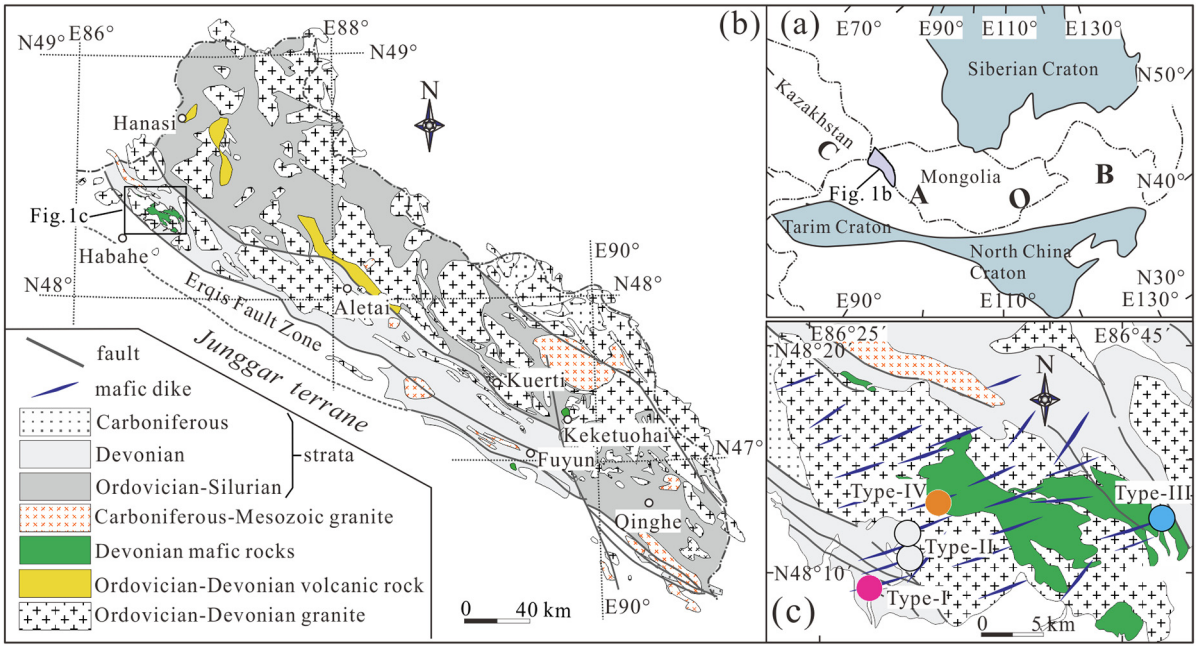

Fig. 1. (a) Simplified regional map showing the location of the Chinese Altai in the Central Asian Orogenic Belt (CAOB); (b) Geological map characterizing the tectonic framework of the Chinese Altai (revised from Sun et al., 2008). (c) Simplified geological maps of the Habahe complex showing rock types and sample locations (Yu et al., 2020).

into the Habahe granite and the surrounding Devonian strata (Fig. 1). These dikes generally show NE-NEE striking with widths of 0.5–5 m and lengths of more than 500 m (Yu et al., 2020). They are mostly massive and aphanitic, and dominantly contain plagioclase and amphibole, both as phenocrysts and groundmass (Fig. A2; Supplemental Table A1). The Habahe mafic dikes are all basaltic and mainly belong to low-K tholeiitic series (Yu et al., 2020). They show systematic variations in trace elements and Sr-Nd-Hf-Pb isotopic compositions from south to north and can be divided into four types (Fig. 1c; Yu et al., 2020): (a) Type-I mafic dikes have narrow ranges of initial $^{87}Sr/^{86}$-Sr ratios (0.7088–0.7095) and $\varepsilon_{Nd}(t)$ values (+3.5 to +3.9) with positive Pb anomalies and low Ba/La ratios (4.24–11.2; Fig. A3), which are interpreted to originate from the mantle source metasomatized by melts from subducted sediments; (b) Type-II mafic dikes show depletion in LREE and are enriched in large ion lithophile elements (LILE; Fig. A3) with high $\varepsilon_{Nd}(t)$ (+6.5–+8.1) and low $(^{87}Sr/^{86}Sr)_i$ (0.7040–0.7049) (Fig. A4), because their mantle source was metasomatized by fluids from the subducted sediments; (c) Type-III mafic dikes show weakly positive Pb anomaly and enrichment in LREE (Fig. A3) and have narrow range of $(^{87}Sr/^{86}Sr)_i$ (0.7036–0.7038) and $\varepsilon_{Nd}(t)$ (+6.7 to +6.9; Fig. A4), which is attributed to the metasomatism of their mantle source by melts from the subducted oceanic crust; (d) Type-IV mafic dikes have lower $(^{87}Sr/^{86}Sr)_i$ ratios (0.7068–0.7070) and $\varepsilon_{Nd}(t)$ values (+0.7 to +1.0) than Type-I mafic dikes but also exhibit positive Pb anomalies and low Ba/La ratios (4.24–11.2; Fig. A3), which are also considered to derive from the mantle source metasomatized by melts from subducted sediments.

3. ANALYTICAL METHODS

All analyses were performed at the State Key Laboratory of Isotope Geochemistry (SKLaBIG), Guangzhou Institute of Geochemistry, Chinese Academy of Sciences (GIG-CAS).

In situ major element analyses were performed on a Cameca SXFiveFE Electron Probe Microanalyzer (EPMA). The operating conditions are: 15 kV accelerating voltage, 20nA beam current, 5 μm beam diameter with peak counting times varying from 8 s to 40 s depending on the intensity of characteristic X-ray line and desired precision. Matrix corrections were based on the PAP (Pouchou and Pichoir) procedure (Pouchou and Pichoir, 1991).

Samples with relatively fresh phenocrysts and groundmass were selected for whole-rock B elemental and isotopic analyses after detailed petrographic observation (Fig. A2). For submarine samples, acid leaching would be an important process before whole-rock B content and isotope analyses. But acid leaching has neglect influences on B isotopic compositions of fresh rocks (Li et al., 2019). On the other hand, the Habahe mafic dikes, emplaced in terrestrial settings, contain abundant amphibole (Fig. A2), which might interact with acid to produce B isotopic fractionation (Fig. A5). Thus, we didn't conduct acid leaching on the studied samples that are relatively fresh. The sample digestion and separation procedures have been described by Wei et al. (2013) in detail. Powder of a sample (about 150 mg) was weighed into a 15 ml polypropylene (PP) centrifuge tube with addition of 150 μl H_2O_2 and 1.5 ml 24 M HF. The tube was tightly sealed and put in a tube holder. Then, it was placed on a hot plate at temperature of ~55 °C for

15 days for sample digestion. The sample solutions were then diluted with B-free Milli-Q deionized water to an HF molarity of 3 M before ion-exchange chromatographic purification. The AG MP-1 strong anion exchange resin was chosen for chromatographic purification to elute B from the collected supernatant. A 2 ml aliquot of elution was transferred into another tube and diluted with 4 ml Milli-Q water. The resultant 6 ml sample solution was used for B concentration measurement by using an ICP-atomic emission spectrometry. The analytical precision for B concentration is generally better than 5% (RSD). Boron isotopic composition was determined by a Neptune-plus MC-ICP-MS and is reported as $\delta^{11}B$, the per mil deviation of $^{11}B/^{10}B$ from that of SRM 951 boric acid. The procedural blanks are <10 ng of B. The replicate measurements of reference material SRM 951 gave $\delta^{11}B$ values of 0.00 ± 0.30‰ (2σ; n = 47) with analyses of independent chemistry. Data of duplicated analyses and reference standards are given in Table 1. External standards of JB-2, JB-3 and B-6 gave B contents (30.5 ppm, 19.1 ppm and 202 ppm, respectively) and $\delta^{11}B$ values (7.48 ± 0.04‰, 6.67 ± 0.04‰ and −2.70 ± 0.05‰, respectively) that are all comparable to the recommended values within error (Table 1; Tonarini et al., 2003; Rosner and Meixner, 2004; Jochum et al., 2016).

4. B ISOTOPE OF THE HABAHE MAFIC DIKES

Boron content and isotope for the Habahe mafic dikes are presented in Table 1 and described with previously reported geochemical data and Sr-Nd-Hf-Pb isotopes (Supplemental Table A2; Cai et al., 2010; Yu et al., 2017a, 2020).

Type-I mafic dikes have variable B contents (5.29–13.4 ppm) with B/Nb ratios from 3.07 to 7.39, and show negative $\delta^{11}B$ values from −6.9‰ to −5.0‰ (Fig. 2). They have $Mg^{\#}$ values of 0.50–0.54 and show variable TiO_2 (0.92–1.12 wt%), Zr (19.9–56.3 ppm), Nb (0.81–2.21 ppm) and Yb (0.75–1.87 ppm) concentrations with narrow range of TiO_2/Yb (0.55–1.23), Nb/Yb (1.08–1.18) and Zr/Yb ratios (26.5–30.1) (Fig. 2). In addition, Type-I samples exhibit large range of LOI (loss of ignition; 3.72–6.01 wt%), which tend to increase with elevation of $\delta^{11}B$ but are poorly correlated with B/Nb (Fig. 2).

Type-II mafic dikes have variable B contents (3.97–9.90 ppm) and $\delta^{11}B$ values from −7.8‰ to −2.7‰, with large range of TiO_2 (0.91–1.10 wt%), Zr (22.6–58.4 ppm), Nb (0.52–1.17 ppm) and Yb (1.63–2.50 ppm) (Fig. 2). They have higher $Mg^{\#}$ (0.57–0.63) and B/Nb (7.07–14.4), and lower LOI (2.27–3.12 wt%), Nb/Yb (0.31–0.47) and Zr/Yb (13.8–23.4) than Type-I mafic dikes with similar TiO_2/Yb (0.44–0.56; Fig. 2). B/Nb and $\delta^{11}B$ of Type-II samples are poorly correlated with LOI (Fig. 2).

Type-III mafic dikes show negative $\delta^{11}B$ values (−7.7‰ to −5.9‰) and have overall low B contents (3.65–6.22 ppm) and B/Nb ratios (2.10–3.93; Fig. 2). These dikes have narrow range of $Mg^{\#}$ (0.63–0.66), LOI (2.10–2.64 wt%), TiO_2 (0.67–0.72 wt%), Zr (62.5–67.1 ppm), Nb (1.58–1.88 ppm) and Yb (1.33–1.48 ppm) with similar TiO_2/Yb (0.49–0.51), Zr/Yb (46.0–48.6) and Nb/Yb (1.16–1.27) ratios (Fig. 2). They show poor correlations between LOI and B/Nb, and LOI and $\delta^{11}B$ (Fig. 2).

Type-IV mafic dikes have higher $\delta^{11}B$ values (−2.9‰ to +3.5‰), B contents (17.0–27.5 ppm) and B/Nb ratios (25.0–40.8) than other three types dikes (Fig. 2). Type-IV samples show similar LOI (2.48–2.90 wt%) that are poorly correlated with B/Nb and $\delta^{11}B$. They have low $Mg^{\#}$ (0.48–0.49), TiO_2 (0.75–0.76 wt%), Zr (23.8–25.8 ppm), Nb (0.64–0.68 ppm) and Yb (2.05–2.17 ppm) with narrow range of TiO_2/Yb (0.35–0.37), Zr/Yb (11.3–12.2) and Nb/Yb (0.30–0.33) ratios (Fig. 2).

5. DISCUSSION

5.1. Influence of crustal evolution processes on B content and isotope

The Habahe mafic dikes exhibit variable B contents and isotopic compositions, which could be induced by crustal processes, such as assimilation of materials from wall rocks, magmatic differentiation and late stage alteration or weathering. The Habahe mafic dikes contain old inherited zircons (417 ± 6 to 1633 ± 5 Ma), indicating some extent of crustal assimilation during magma emplacement into the Devonian strata (Yu et al., 2020). The continental materials exhibit a large range of B contents (2–101 ppm) and isotopic compositions (e.g., $\delta^{11}B = -20‰$ to +28‰; Trumbull and Slack, 2018). The Habahe mafic dikes may have undergone assimilation of similar crustal materials. However, these mafic dikes all show low K_2O contents, which are poorly correlated with B/Nb, $\delta^{11}B$ (Fig. 2) and Sr-Nd-Hf-Pb isotopes (Yu et al., 2020). This indicates the insignificant role of the crustal contamination in modifying their geochemical compositions (Yu et al., 2020).

The Habahe mafic dikes show variable $Mg^{\#}$ values (Fig. 2), suggesting different extents of fractional crystallization of mafic minerals, such as olivine, clinopyroxene and orthopyroxene. However, fractional crystallization of these mafic minerals will not significantly change B isotopic compositions in residual melts because B is strongly incompatible in these minerals (Trumbull and Slack, 2018). In contrast, arc magmas have high content of H_2O and will undergo degassing with exsolution of fluids after their emplacement into the crust (Plank et al., 2013), which can potentially cause a decrease in $\delta^{11}B$ values in the residual magma due to different boron coordination numbers (III-IV) in melt and fluid (Wunder et al. 2005; Kowalski et al. 2013). Type-IV mafic dikes have lower $Mg^{\#}$ values than other three dike types, corresponding to more evolved composition. However, Type-IV mafic dikes show much higher $\delta^{11}B$ than other samples, which is inconsistent with a trend of decreasing $\delta^{11}B$ values due to degassing during magmatic evolution. In addition, each type of the Habahe mafic dikes shows a poor correlation between B/Nb and $Mg^{\#}$ (Fig. 2), denoting that fractional crystallization or degassing processes cannot account for the variation of B content and isotopic compositions of these dikes.

Due to high mobility in fluids, B content and isotope of rocks can be modified during late stage alteration and weathering (Gaillardet and Lemarchand, 2018).

Table 1
Whole-rock geochemical compositions and B-Sr-Nd-Hf-Pb isotopes of the Habahe mafic dikes.

Sample	Type	$Mg^{\#}$	LOI (wt%)	Nb(ppm)	B(ppm)	B/Nb	$\delta^{11}B$(‰)	2σ	$(^{87}Sr/^{86}Sr)_i$	$\varepsilon_{Nd}(t)$	$\varepsilon_{Hf}(t)$	$(^{206}Pb/^{204}Pb)_t$	$(^{207}Pb/^{204}Pb)_t$	$(^{208}Pb/^{204}Pb)_t$
HB15-7	I	0.54	6.01	0.81	5.29	6.56	−4.96	0.06	0.7095	3.8	12.1	18.018	15.538	37.981
HB15-8	I	0.50	3.46	1.94	9.77	5.04	−6.86	0.04	0.7089	3.5	9.50	18.034	15.551	37.991
HB15-9	I	0.52	4.54	1.92	5.90	3.07	−6.33	0.05	0.7094	3.8	10.0	18.000	15.533	37.937
HB15-10	I	0.50	5.24	1.81	13.4	7.39	−6.19	0.05	0.7088	3.9	9.90	17.971	15.526	37.860
BH1-7	II	0.60	2.61	0.69					0.7048	8.1	14.2	17.839	15.494	37.797
BH1-9	II	0.60	2.29	1.17					0.7041	7.7	15.4	17.715	15.484	37.739
HB15-32	II	0.63	3.12	0.56	4.28	7.70	−6.24	0.06	0.7041	7.4	14.6	17.809	15.492	37.785
HB15-33	II	0.59	2.27	0.52	3.97	7.71	−3.81	0.05	0.7049	7.3	13.9	17.821	15.495	37.777
HB15-34	II	0.63	3.08	0.59	4.18	7.07	−7.79	0.07	0.7040	7.4	14.8	17.814	15.494	37.788
HB15-35	II	0.57	2.36	0.69	9.90	14.4	−2.74	0.05	0.7047	6.5	13.4	17.779	15.493	37.763
HB15-229	III	0.65	2.64	1.70	3.87	2.29	−7.49	0.08	0.7038	6.7	14.6	17.871	15.488	37.625
HB15-230	III	0.64	2.58	1.68	3.99	2.37	−7.70	0.10	0.7036	6.7	14.8	17.971	15.488	37.642
HB15-231	III	0.66	2.46	1.58	6.22	3.93	−6.15	0.09	0.7036	6.9	14.6	17.883	15.485	37.611
HB15-232	III	0.63	2.37	1.73	3.65	2.10	−5.87	0.12	0.7038			18.001	15.491	37.610
HB12	IV	0.49	2.90	0.68	17.0	25.0	−2.85	0.04	0.7068	1.0	5.50	18.402	15.553	38.299
HB14	IV	0.48	2.72	0.64	26.1	40.8	3.48	0.05	0.7068	0.7	7.70	18.101	15.527	38.163
HB15	IV	0.48	2.77	0.68	27.5	40.4	3.05	0.04	0.7070	0.9	7.80	18.001	15.522	38.188
HB15-10R	*DP*				*14.7*		*−6.08*	*0.04*						
HB14R	*DP*				*25.3*		*3.34*	*0.04*						
JB-2	*SD*				*30.5*		*7.48*	*0.04*						
JB-3	*SD*				*19.1*		*6.67*	*0.04*						
B-6	*SD*				*202*		*−2.70*	*0.05*						

Note: Rock type abbreviation: I = Type-I mafic dike; II = Type-II mafic dike; III = Type-III mafic dike; IV = Type-IV mafic dike. The geochemical compositions and Sr-Nd-Hf-Pb isotopes of the Habahe mafic dikes are from Cai et al. (2010) and Yu et al. (2017a, 2020). Italic font shows duplicate (DP) and standard (SD) analyses. t = 360 Ma. The recommended content and isotope for JB-2, JB-3 and B-6 are 29.98 ± 0.74, 20.0 ± 2 and 205.8 ± 7.5 ppm, and 7.25 ± 0.64‰, 6.51 ± 0.67‰ and −2.76 ± 0.48‰ (Tonarini et al., 2003; Rosner and Meixner, 2004; Jochum et al., 2016).

Table 2
Modelling parameters in partial melting of the mantle wedge.

Elements	Nb(ppm)	Zr(ppm)	Yb(ppm)	TiO_2(wt%)
Endmember	Concentrations			
EM	0.713	10.50	0.441	0.279
DM	0.080	4.500	0.401	0.171
Mineral (percentage)	Partition coefficients (KD)			
Ol[1] (52%)	0.0001	0.001	0.05	0.011
Opx[2] (27%)		0.014	0.092	0.10
Cpx[3] (18%)	0.0028	0.045	0.22	0.21
Spl[4,5] (3%)	0.0006	0.0081	0.0045	0.048

Note: [1]Adam and Green (2006); [2]Salters and Longhi (1999); [3]Lundstrom et al. (1998); [4]Elkins et al. (2008); [5]Shaw (2000). Ol – olivine; Opx – orthopyroxene; Cpx – clinopyroxene; Spl – spinel; DM – depleted mantle. The enriched mantle (EM) are represented by primitive mantle in Sun and McDonough (1989).

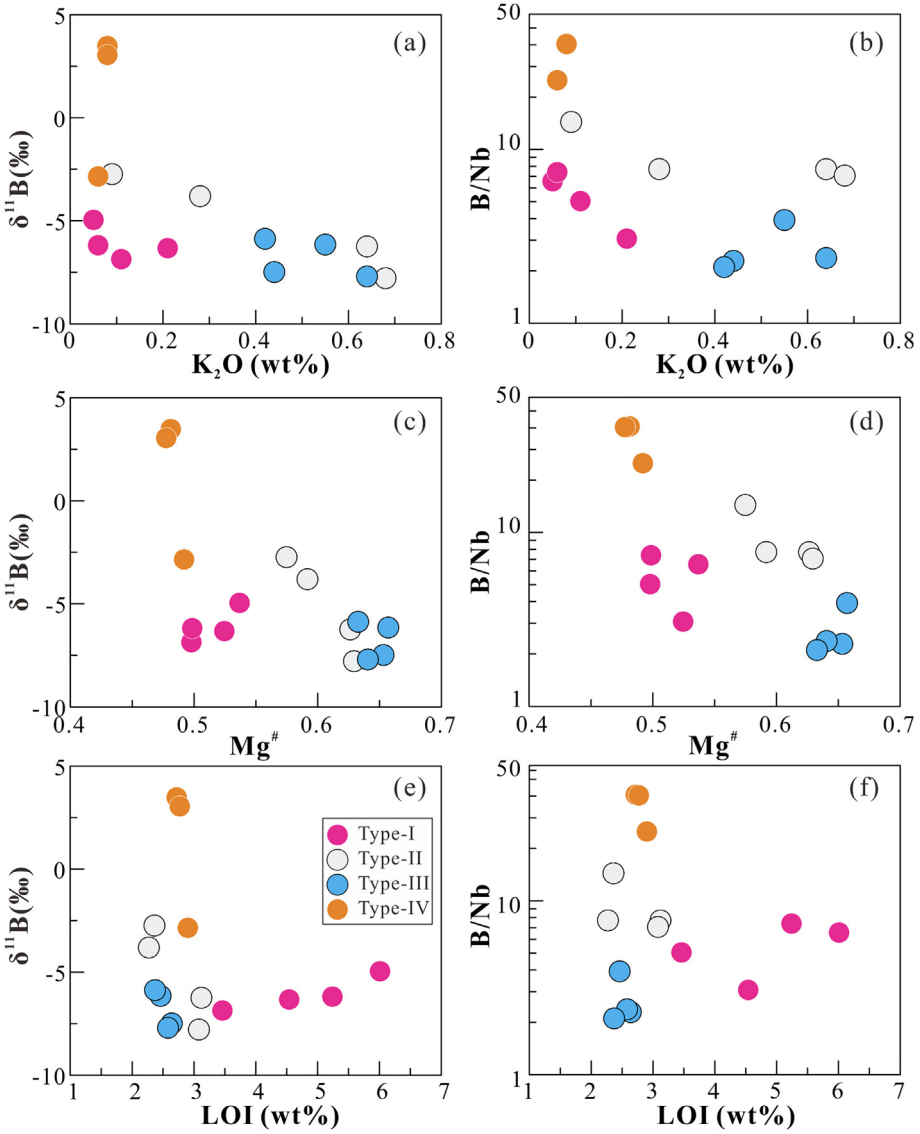

Fig. 2. Diagrams of (a) $\delta^{11}B$ (‰) vs. K_2O, (b) B/Nb vs. K_2O, (c) $\delta^{11}B$ (‰) vs. $Mg^{\#}$, (d) B/Nb vs. $Mg^{\#}$, (e) $\delta^{11}B$ (‰) vs. LOI, and (f) B/Nb vs. LOI for the Habahe mafic dikes. LOI – loss of ignition.

Type-II, -III and -IV mafic dikes contain fresh phenocrysts and groundmass of plagioclase and amphibole (Fig. A2) and show relatively low LOI (Fig. 2). This indicates that these samples have not undergone strong alteration and weathering. In addition, B/Nb and $\delta^{11}B$ of these samples are poorly correlated with LOI (Fig. 2e, f), suggesting insignificant modification of alteration and weathering on their B composition. In contrast, Type-I mafic dikes have wide range of LOI (Fig. 2), and some fine-grained amphiboles and plagioclases have been partially altered (Fig. A2), indicating slight alteration. These samples tend to show slightly higher $\delta^{11}B$ values with increasing LOI (Fig. 2). This is inconsistent with B isotope lightening trend during weathering because ^{10}B tends to be enriched in clay minerals formed by weathering (Spivack et al., 1987; Gaillardet and Lemarchand, 2018). The influence of alteration on the B content and isotopic composition of rocks are determined by fluid compositions (Thompson and Melson, 1970; Spivack and Edmond, 1987; Gaillardet and Lemarchand, 2018; Xu et al., 2021). For example, alteration products formed by seawater will show strong enrichment of boron and heavy B isotope due to high B and $\delta^{11}B$ in seawater (Thompson and Melson, 1970; Spivack and Edmond, 1987; Gaillardet and Lemarchand, 2018), while alteration by external fluids in terrestrial settings may increase B content and decrease $\delta^{11}B$ in residual products (Xu et al., 2021). Type-I mafic dikes show poor correlation between LOI and B/Nb and have lower B/Nb ratios than Type-II and -IV mafic dikes (Fig. 2), which contradicts a significant enrichment of B during the alteration process. Therefore, B content and isotopic composition of the Habahe mafic dikes should have not been significantly modified by the late stage alteration and weathering.

5.2. B isotopic features of subduction components

The Habahe mafic dikes have low K_2O and positive $\varepsilon_{Hf}(t)$ values (Figs. 2, A4), indicating their origination from partial melting of the depleted mantle wedge during subduction of the Junggar Ocean (Yu et al., 2020). Moreover, they have much higher B contents (3.65–27.5 ppm) and B/Nb ratios (2.10–40.8) than MORBs (B < 2.5 ppm; B/Nb = 0.15–1.05; Marschall et al., 2017), indicating addition of B from the subducted slab into their mantle sources. Different $\delta^{11}B$ values of these mafic dikes reflect variable B isotopic compositions for different subduction components.

5.2.1. B isotopically light melts from subducted sediments and oceanic crust

B can undergo significant isotopic fractionation during dehydration of the subducted slab because ^{11}B prefers trigonal coordination in fluids, while ^{10}B can be retained in tetrahedral coordination in the residual rocks (Hervig et al., 2002; Kowalski and Wunder, 2018). In contrast, slab melting may play insignificant role in B isotopic fractionation during the subduction because B prefers tetrahedral co-ordination in magma (Maner and London, 2018; Sugden et al., 2020).

Based on trace elements and Sr-Nd-Hf-Pb isotopes, Type-I mafic dikes have been interpreted as derivation from the mantle source with involvement of melts from subducted sediments, while Type-III mafic dikes were derived from a depleted mantle source metasomatized by melts from subducted oceanic crust (Fig. 3; Yu et al., 2017a, 2020). Type-I and -III mafic dikes all show negative $\delta^{11}B$ values (−7.7‰ to −5.0‰; Table 1), indicating that components from the subducted sediments and oceanic crust involved in the mantle sources have light B isotopic compositions (Fig. 4). It is noteworthy that Type-I mafic dikes have $\delta^{11}B$ values similar to the metamorphosed terrigenous sediments, such as those in California and Lago di Cignana, Italy ($\delta^{11}B = -15‰$ to −7‰ in tourmalines; Bebout and Nakamura, 2003), but are lower than marine sediments ($\delta^{11}B = -4‰$ to +3‰; Spivack et al., 1987) and mixed marine-terrigenous sediments from Syros, Greece ($\delta^{11}B = -1.6‰$ to +0.9‰ in tourmaline mantles; Marschall et al., 2008). In the Chinese Altai, the early Paleozoic accretionary complex is dominantly composed of continental clastic sediments (Jiang et al., 2010, 2016), indicating that the subducted sediments involved in the mantle source for Type-I mafic dikes may be mainly composed of terrigenous sediments with light B isotopic compositions. On the other hand, the $\delta^{11}B$ values of Type-III mafic dikes (−7.7‰ to −5.9‰; Fig. 4) resemble those of the subducted oceanic crust in the Mariana arc ($\delta^{11}B = -6 \pm 4‰$; Pabst et al., 2012), suggesting that the subducted oceanic crust in the Chinese Altai also has a similarly light B isotopic composition.

Both the Type-I and -III mafic dikes show low B/Nb ratios (Fig. 3; Table 1), suggesting low B abundance of the melts derived from the subducted sediments and oceanic crust. B can be efficiently removed (>80%) from the subducted sediments and oceanic crust during slab dehydration at the fore-arc (Scambelluri et al., 2004; Konrad-Schmolke and Halama, 2014; Ryan and Chauvel, 2014). The concomitant B isotopic fractionation will leave light B isotopic compositions for the residual slab (Bebout and Nakamura, 2003; Pabst et al., 2012; Ryan and Chauvel, 2014). Such processes should be responsible for the low B abundance and light B isotope of the subducted sediments and oceanic crust in the Chinese Altai.

5.2.2. B isotopically heavy fluids from subducted serpentinite

According to trace elements and Sr-Nd-Hf-Pb isotopes, the mantle source for Type-IV mafic dikes was metasomatized by melts from subducted sediments (Yu et al., 2020). However, the Type-IV mafic dikes have much higher $\delta^{11}B$ values (−2.85‰ to +3.48‰) than Type-I mafic dikes ($\delta^{11}B = -6.9‰$ to −5.0‰; Fig. 2), inconsistent with the light B isotopic features of melts from the subducted sediments. Based on the B abundance and B isotope, Sugden et al. (2020) suggested that the mantle sources for the Armenian post-collisional volcanic rocks were previously metasomatized by melts derived from the mixed marine-terrigenous sediments. It is noteworthy that B/Nb of Type-I mafic dikes (3.07–7.39) and the Armenian post-collisional volcanic rocks (0.03–0.25) are all much lower than the Type-IV mafic dikes (25.0–40.8; Table 1). Thus, high B/Nb ratios and heavy B isotopic compositions of Type-IV mafic dikes suggest that there may be another

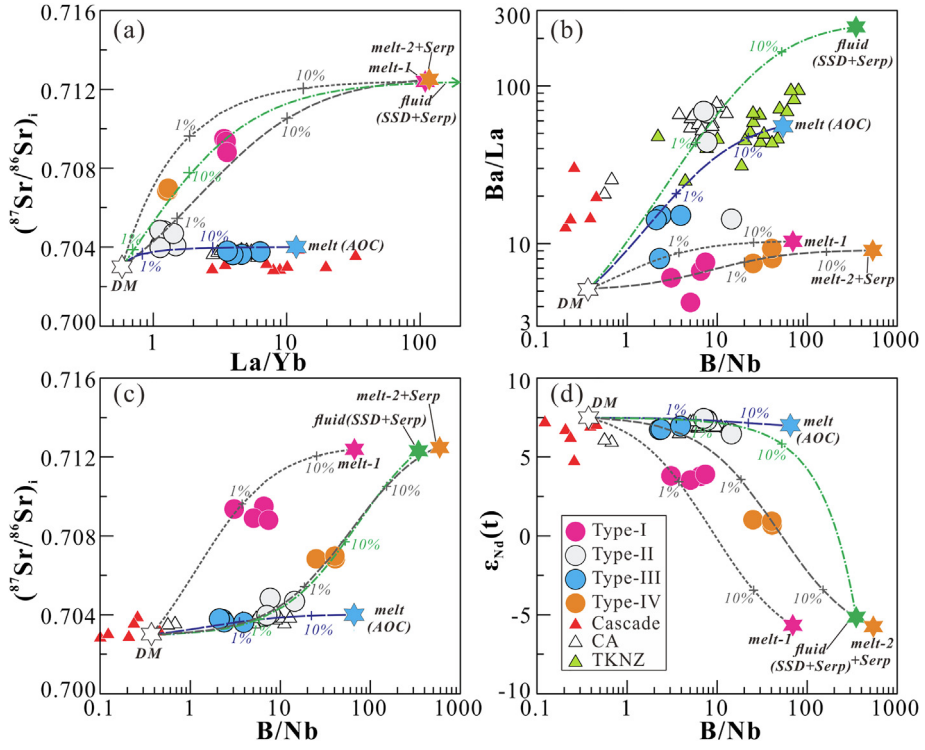

Fig. 3. Diagrams of (a) $(^{87}Sr/^{86}Sr)_i$ vs. La/Yb, (b) Ba/La vs. B/Nb, (c) $(^{87}Sr/^{86}Sr)_i$ vs. B/Nb, and (d) $\varepsilon_{Nd}(t)$ vs. B/Nb for the Habahe mafic dikes. The mantle wedge is represented by the depleted mantle (DM) from Salters and Stracke (2004). The subducted sediments (SSD) are represented by the sedimentary rocks of early Paleozoic accretionary complex in the Chinese Altai (Chen and Jahn, 2002). Altered oceanic crust (AOC) is represented by N-MORB with trace elements from Sun and McDonough (1989) and radiogenic $^{87}Sr/^{86}Sr$ of 0.7040. Serpentinite is represented by subducted serpentinite (dunite) in Deschamps et al. (2013). B contents of the subducted sediments and altered oceanic crust are assumed as 11.6 ppm and 8.4 ppm, respectively. Fluid compositions are calculated with partition coefficients from Kessel et al. (2005) under 4 GPa and 700 ℃. Melts from subducted sediments and altered oceanic crust are calculated by batch melting model. Melt-1 and melt-2 represent the melts from subducted sediments in two stages melting processes (Yu et al., 2020). We assume that 80% B, 80% Sr, 5% Nd, 5% La, 5% Ba, 1% Hf and 1% Yb have escaped from subducted sediments during the first stage melting, which reflects significant loss of B and Sr for the subducted sediments at shallow depth of subduction zone (Yu et al., 2020). B content of melts from the subducted sediments and oceanic crust are calculated with partition coefficient from Kessel et al. (2005) because B is strongly incompatible in both dehydration and melting of subducted slab. Dehydration and melting conditions and modelling parameters are summarized in Supplemental Table A3. Data of IAB from the Cascade, Central America (CA) and Tonga-Kermadec-New Zealand (TKNZ) are compiled from Leeman et al. (2004, 2017) and Tonarini et al. (2007).

subduction component involved in their mantle source in addition to melts from the subducted sediments. B may be transferred into the deep mantle by some hydrous minerals (e.g., phengite and antigorite) that remain stable at high pressure and temperature (Kowalski and Wunder, 2018). As a major rock-forming mineral hosting B at deep subduction depth, phengite is expected to have negative $\delta^{11}B$ values because mica would preserve isotopically light B when it interacts with fluids during the early stage of subduction at shallow depth (Konrad-Schmolke et al., 2016; Kowalski and Wunder, 2018). Thus, melts from the breakdown of phengite during the melting of subducted sediments may inherit light B isotopic compositions. In addition, phengite is also enriched in K and Ba, its breakdown will result in high K_2O and Ba/La ratios in the melts. Therefore, input of melts from the breakdown of phengite cannot explain high $\delta^{11}B$ values and low K_2O and Ba/La in Type-IV mafic dikes (Figs. 2, 3). On the other hand, serpentinite can have variable B isotopic compositions depending on their genesis (Deschamps et al., 2013; Yamada et al., 2019; Martin et al., 2020). The mantle-wedge serpentinites produced via hydration of peridotite by subducted crust-derived metamorphic fluids at the base of the mantle wedge are expected to have relatively light B isotopic compositions ($\delta^{11}B = -14.4‰$ to $+10‰$; Hyndman and Peacock, 2003; Scambelluri and Tonarini, 2012; Martin et al., 2016). In contrast, slab serpentinites commonly have heavy B isotopic compositions ($\delta^{11}B = +12‰$ to $+34‰$) due to their formation by reaction of peridotite with seawater from the oceanic lithosphere (Martin et al., 2016; 2020; Yamada et al., 2019). Thus, the slab serpentinite can retain the signature of seawater-derived isotopically heavy B at subduction depth of 80–140 km (Deschamps et al., 2013; Konrad-Schmolke and Halama, 2014; Martin et al., 2020). Dehydration of antigorite will produce fluids with high B concentrations and highly positive $\delta^{11}B$ values (Deschamps et al., 2013; Konrad-Schmolke and Halama, 2014). Since antigorite has much lower content of Ba (~5.72 ppm; Deschamps et al., 2013) than phengite (e.g., BaO = 0.2–1.6 wt%; Catlos and Sorensen, 2003),

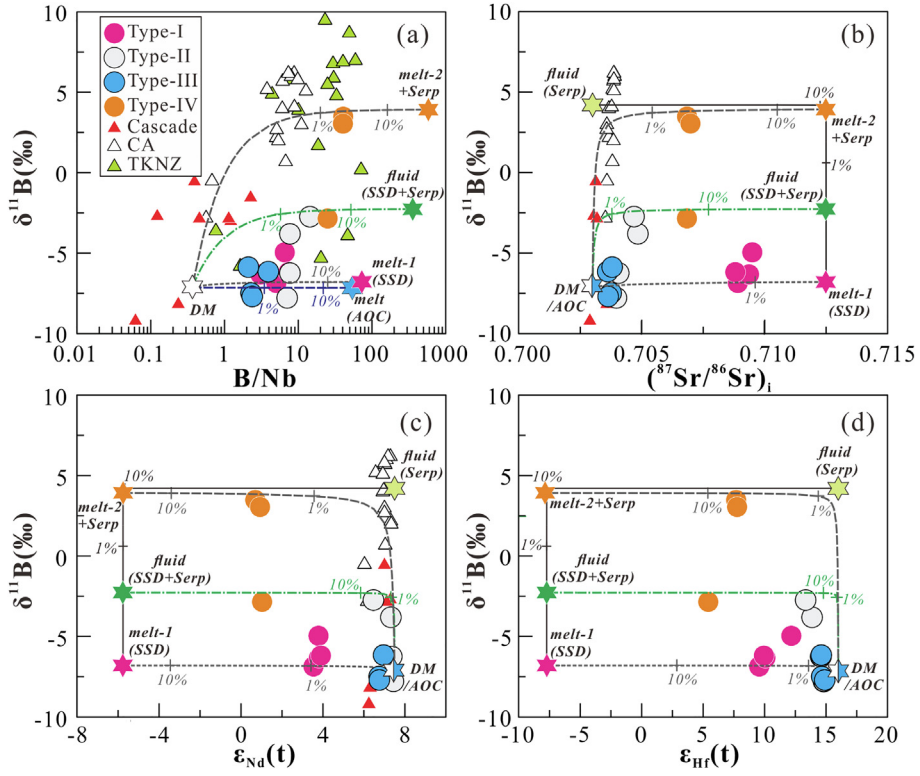

Fig. 4. Diagrams of (a) $\delta^{11}B$ vs. B/Nb, (b) $\delta^{11}B$ vs. $(^{87}Sr/^{86}Sr)_i$, (c) $\delta^{11}B$ vs. $\varepsilon_{Nd}(t)$, and (d) $\delta^{11}B$ vs. $\varepsilon_{Hf}(t)$ for the Habahe mafic dikes. $\delta^{11}B$ of the subducted sediments and altered oceanic crust are assigned as −6.8 and −7.1, respectively, because they should have undergone loss of B at shallow subduction depth. Dehydration and melting conditions and modelling parameters for the subducted sediments (SSD), serpentinite (Serp) and altered oceanic crust (AOC) and the middle Paleozoic mantle wedge (DM) are same with Fig. 3 and summarized in Supplemental Table A3. Data of IABs from the Cascade, Central America (CA) and Tonga-Kermadec-New Zealand (TKNZ) are compiled from Leeman et al. (2004, 2017) and Tonarini et al. (2007).

breakdown of antigorite will generate fluids with relatively low Ba/La ratios (Fig. 3b). In addition, fluids from the Sr and Nd-depleted slab serpentinite will have much lower Sr and Nd concentrations (Plank and Langmuir, 1998; Deschamps et al., 2013) than melts from subducted sediments and thus cannot significantly change Sr-Nd isotopes of the mantle wedge (Supplemental Table A3). Therefore, high $\delta^{11}B$, low Ba/La and enriched Sr-Nd isotopic features in Type-IV mafic dikes suggest that their mantle sources should be metasomatized by hybridization agents including fluids from slab serpentinite (~0.7%) and melts from subducted sediments (~1.3%; Figs. 3 and 4).

Type-II mafic dikes have been attributed to the metasomatism of their mantle source by fluids from subducted sediments (Fig. 3; Yu et al., 2020). Two samples (HB15-32, HB15-34) of Type-II mafic dikes are similar to Type-I mafic dikes in their low $\delta^{11}B$ values (−7.8‰ to −6.2‰) and B/Nb ratios (7.01–7.70) (Table 1; Fig. 2). This is consistent with the involvement of fluids originated from the subducted sediments that have low B abundance and light B isotopic compositions (Fig. 4). The other two samples (HB15-33, HB15-35) have higher $\delta^{11}B$ (−3.8‰ to −2.7‰) and B/Nb ratios (7.71–14.4; Fig. 2) than the Type-I mafic dikes, suggesting high B content and heavy B isotopic compositions for the subduction components in their mantle source. Overall, Type-II mafic dikes show variable $\delta^{11}B$, which resembles the subducted oceanic crust in the Mariana arc ($\delta^{11}B = -6 \pm 4‰$; Pabst et al., 2012). The subducted oceanic crust has much lower B content (~8 ppm; Pabst et al., 2012) than the subducted sediments (~30.9 ppm; Nakano and Nakamura, 2001), implying that the fluids from the subducted oceanic crust may have relatively low B/Nb. Thus, input of the fluids from the subducted oceanic crust in the mantle source might not explain high B/Nb ratios in some samples of Type-II mafic dikes. Dehydration of phengite can generate high $\delta^{11}B$ and B/Nb fluids due to boron isotope fractionation between phengite and fluid (Wunder et al., 2005), but is inconsistent with low K_2O of Type-II mafic dikes (Fig. 2). Alternatively, variable $\delta^{11}B$ of Type-II mafic dikes would be attributed to their complex mantle sources, which might be metasomatized by minor amounts of slab serpentinite-derived fluids (~0.06%), in addition to fluids from subducted sediments (~1.44%; Figs. 3 and 4).

5.2.3. Implications for B recycling in subduction zone

Island arc basalts are characterized by variable B concentrations (1.3–37 ppm) and isotopic compositions ($\delta^{11}B = -9‰$ to +16‰; De Hoog and Savov, 2018). This reflects complicated metasomatism in the mantle wedge by different subduction components from subducted sediments, altered oceanic crust and/or serpentinite (Ishikawa

and Tera, 1999; Deschamps et al., 2013; De Hoog and Savov, 2018). Because terrestrial sediments and altered oceanic crust have distinct B isotopic compositions ($\delta^{11}B = -16‰$ to $-3‰$ and $-4‰$ to $+25‰$, respectively; Spivack et al., 1987; Ishikawa and Nakamura, 1993; Marschall et al., 2008, 2017), it is proposed that B isotopic variation in island arc basalts would be caused by the input of different fluids into the mantle wedge, which were derived from dehydration of subducted sediment/altered oceanic crust in varying proportions (Ishikawa and Tera, 1999). On the other hand, the subducted sediments and oceanic crust would undergo significant loss of B (e.g., >80%; You et al., 1995, 1996; Savov et al., 2007) at the fore-arc, and the residual slab should have light B isotopic compositions due to isotopic fractionation during slab dehydration (Bebout and Nakamura, 2003; Pabst et al. 2012; Ryan and Chauvel, 2014). Hence, heavy B isotopic compositions of arc magmas were explained by involvement of fluids from dehydration of slab serpentinite in the mantle wedge (Deschamps et al., 2013; Konrad-Schmolke and Halama, 2014). The second scenario is typically shown by the Habahe mafic dikes in this study. Type-I and -III mafic dikes exhibit similarly low B/Nb and light B isotopic compositions (Fig. 2) although they originated from mantle sources metasomatized by melts from the subducted sediments and the subducted oceanic crust, respectively. This demonstrates that the subducted sediments and the oceanic crust only have a slight amount of B after the loss of B at the fore-arc depth. However, Type-IV mafic dikes and some samples of Type-II mafic dikes have high B/Nb and heavy B isotopic compositions, which would be result from the input of fluids from the slab serpentinite in their mantle sources. Thus, B isotope can be efficiently used to identify whether the fluids from slab serpeninite is involved in the mantle wedge during the subduction but would be reluctant for distinguishing the components from subducted sediments and oceanic crust.

5.3. Influence of subduction components on melting in the mantle wedge

5.3.1. Different melting processes for mantle sources of the Habahe mafic dikes

IABs are typically characterized by enrichment of LREE and LILE and depletion of high field strength elements (HFSE) and heavy REE (HREE), because these elements will be retained by rutile, zircon or garnet in the subducted slab (e.g., Klimm et al., 2008). Thus, HFSE and HREE in IAB are mainly contributed by the mantle wedge instead of the subduction components and can be used to evaluate the melting process in the mantle wedge (Kelley et al., 2006; 2010). HFSE (Nb, Zr, Ti) show different incompatibilities with Yb during melting of the mantle peridotite. For example, Nb and Zr tend to be more incompatible than Yb (Lundstrom et al., 1998; Salters and Longhi, 1999; Shaw, 2000; Elkins et al., 2008), while Ti shows a similar partition coefficient to Yb during mantle melting (Lundstrom et al., 1998; Salters and Longhi, 1999; Shaw, 2000; Adam and Green, 2006; Elkins et al., 2008). TiO_2/Yb ratios in IAB will not be significantly changed by different degree melting of the mantle wedge and resemble their mantle sources (Kelley et al., 2006). Except for one Type-I sample, the Habahe mafic dikes all show relatively constant and low TiO_2/Yb ratios (Fig. 5), indicating that they were all produced by partial melting of similarly depleted mantle sources. The Habahe mafic dikes show variable Zr/Yb and Nb/Yb ratios that poorly correlate with $\varepsilon_{Hf}(t)$ and $\varepsilon_{Nd}(t)$ values (Fig. 5a-d), indicating that these dikes were formed through varying degrees melting of the depleted mantle wedge (Fig. 5e-f).

5.3.2. Role of water flux in melting of the mantle source

The Habahe mafic dikes emplaced simultaneously within a short distance (<20 km) and should be produced by partial melting of the mantle wedge with the same subduction regime. This denotes that variable extents melting of their mantle sources were not caused by differences in factors of the mantle wedge thermal structure (England and Katz, 2010; Perrin et al., 2018), slab dip angle and speed (Grove et al., 2009) or the upper plate thickness (Turner and Langmuir, 2015a, b; Turner et al., 2016).

The mantle sources of the Habahe mafic dikes are metasomatized by different subduction components, including fluids and melts (Fig. 3), which show different capacities in lowering the solidus of peridotite (e.g., Grove et al., 2006; Mallik et al., 2015). Silica melts may lower the solidus line of peridotite to 1100–1150 °C at 2–3 GPa (Mallik et al., 2015), while addition of water can cause melting of peridotite at ~810–850 °C at 2–3 GPa (Grove et al., 2006). As discussed above, the mantle source for Type-II mafic dikes was metasomatized by fluids from subducted sediments (Fig. 4), while that of Type-IV mafic dikes was mainly metasomatized by melts from subducted sediments and fluids from slab serpentinite. Consequently, the mantle source for the former should have been melted at larger degree than that for the latter. However, Type-II mafic dikes show higher Zr/Yb and Nb/Yb ratios than Type-IV mafic dikes, indicating lower degree melting of the mantle source (Fig. 5). Thus, the different extent melting of the mantle wedge cannot also be explained by input of different forms of subduction components (fluids and melts).

The Habahe mafic dikes show variable B/Nb ratios, which has been proposed as proxy denoting input of different amounts of water into the mantle wedge (Konrad-Schmolke et al., 2016; Leeman et al., 2017; Cooper et al., 2020). B and H_2O are highly incompatible during dehydration and melting of subducted slab, while Nb shows low mobility in both fluids and melts due to retainment by residual rutile in subducted slab (Hermann and Rubatto, 2009; De Hoog and Savov, 2018). Therefore, the subducted slab can contribute significant B and H_2O to arc magmas, while its contribution of Nb is negligible. Due to extreme depletion of B and H_2O in the primitive mantle wedge, high B and H_2O in IAB dominantly come from the subducted slab (Plank et al., 2013; Marschall et al., 2017; De Hoog and Savov, 2018). On the other hand, B, H_2O and Nb all show similar incompatibility during melting of the mantle peridotite and evolution of the mafic magmas (Brenan et al., 1998; Marschall et al., 2007; Manea et al., 2014). B/Nb ratios in IAB will not significantly change with vary-

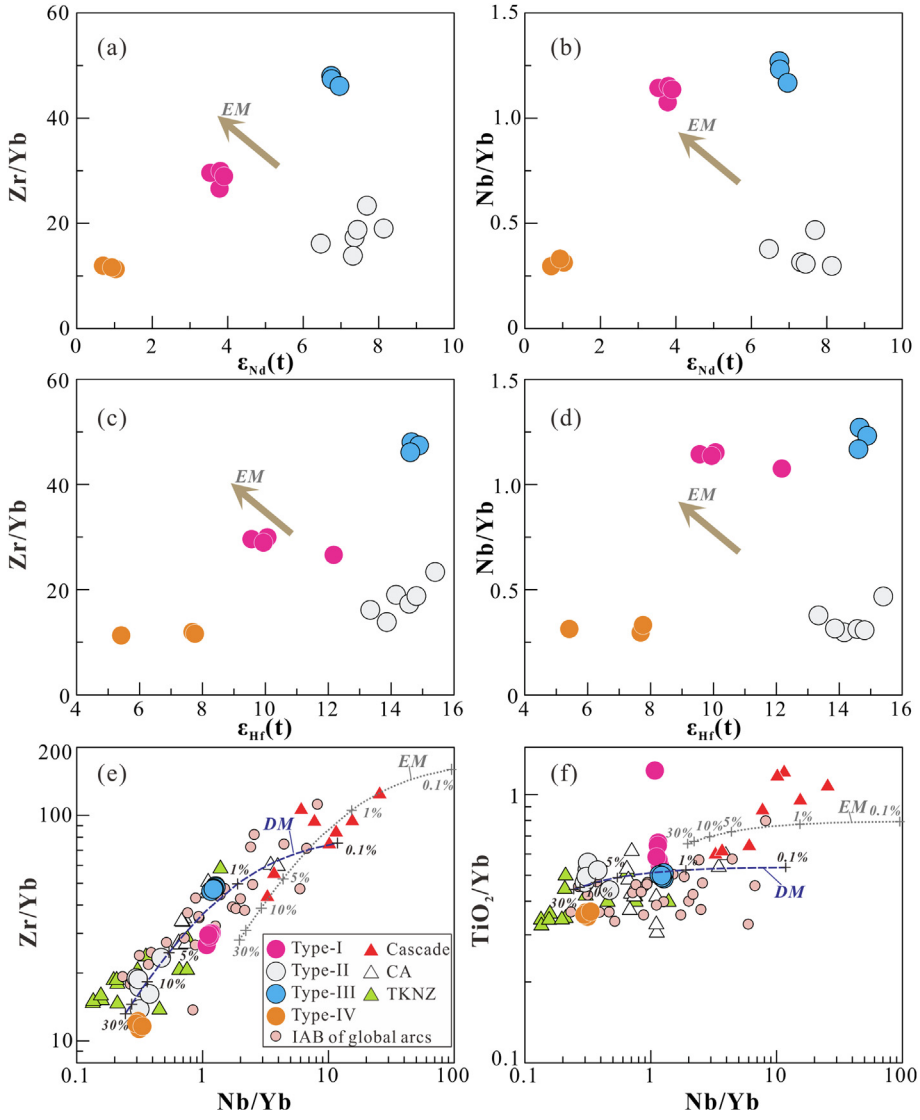

Fig. 5. Diagrams of (a) Zr/Yb vs. $\varepsilon_{Nd}(t)$, (b) Nb/Yb vs. $\varepsilon_{Nd}(t)$, (c) Zr/Yb vs. $\varepsilon_{Hf}(t)$, (d) Nb/Yb vs. $\varepsilon_{Hf}(t)$, (e) Zr/Yb vs. Nb/Yb, and (f) TiO_2/Yb vs. Nb/Yb for the Habahe mafic dikes. DM – depleted mantle. The enriched mantle (EM) are represented by the primitive mantle in Sun and McDonough (1989). The parameters used in the mantle melting processes are compiled in Table 2. Data of IAB from the Cascade, Central America (CA) and Tonga-Kermadec-New Zealand (TKNZ) are compiled from Leeman et al. (2004, 2017) and Tonarini et al. (2007). Data of IABs from global arcs are compiled from database in Turner and Langmuir (2015a).

ing degrees of melting of the mantle wedge or later stage magmatic differentiation (Fig. 2; Manea et al., 2014) and can thus be used as proxy of water flux (Konrad-Schmolke et al., 2016; Leeman et al., 2017; Cooper et al., 2020). In fact, co-variation of water flux beneath arcs and B/Nb in IAB has been observed in the Kamchatka (Ishikawa et al., 2001; Konrad-Schmolke et al., 2016) and Lesser Antilles arcs (Cooper et al., 2020). Thus, the large range of B/Nb ratios in the Habahe mafic dikes indicates input of variable amounts of water from the subducted slab into the mantle wedge, which could cause different degrees of melting of their mantle sources.

Type-II and -IV mafic dikes have higher B/Nb ratios than other mafic samples (Fig. 2), due to involvement of fluids from the slab serpentinite in their mantle sources (Fig. 4). Dehydration of serpentinite can introduce large amount of water into the mantle wedge (Deschamps et al., 2013) and should cause high degree melting of the mantle peridotite (Gaetani and Grove, 1998; Till et al., 2012). This process is shown by low Nb/Yb and Zr/Yb for Type-II and -IV mafic dikes, suggesting their formation through high degree melting (F = 10–20 %) of the depleted mantle source (Fig. 6). On the other hand, Type-I and -III mafic dikes show overall lower B/Nb ratios than Type-II and -IV mafic dikes (Fig. 2) because their mantle sources were mainly metasomatized by melts from subducted sediments and oceanic crust, respectively (Fig. 3). Low B/Nb ratios of Type-I and -III mafic dikes imply low water content in their mantle sources, which has caused low degree melting (1–5 %) processes, responsible for high Zr/Yb and Nb/Yb ratios in these samples (Fig. 6). Therefore, B/Nb ratios of these samples are negatively correlated with

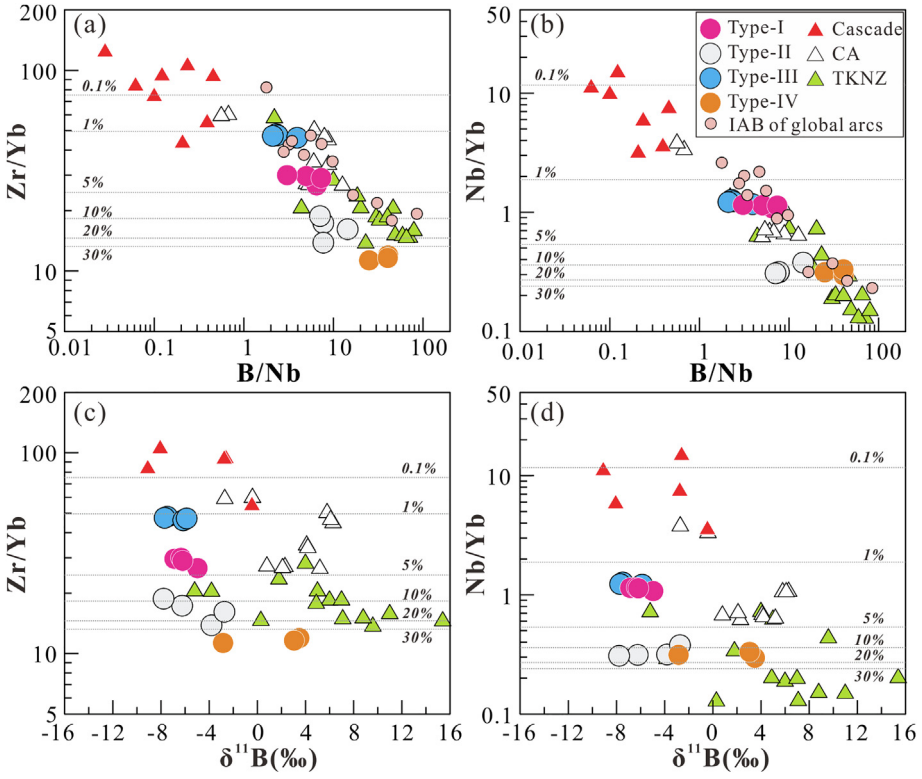

Fig. 6. Diagrams of (a) Zr/Yb vs. B/Nb, (b) Nb/Yb vs. B/Nb, (c) Zr/Yb vs. $\delta^{11}B$, and (d) Nb/Yb vs. $\delta^{11}B$ for the Habahe mafic dikes. The gray dashed lines represent different extent melting of the depleted mantle. The parameters used in the mantle melting processes are compiled in Table 2. Data of IAB from the Cascade, Central America (CA) and Tonga-Kermadec-New Zealand (TKNZ) are compiled from Leeman et al. (2004, 2017) and Tonarini et al. (2007). Data of IABs from global arcs are compiled from database in Turner and Langmuir (2015a).

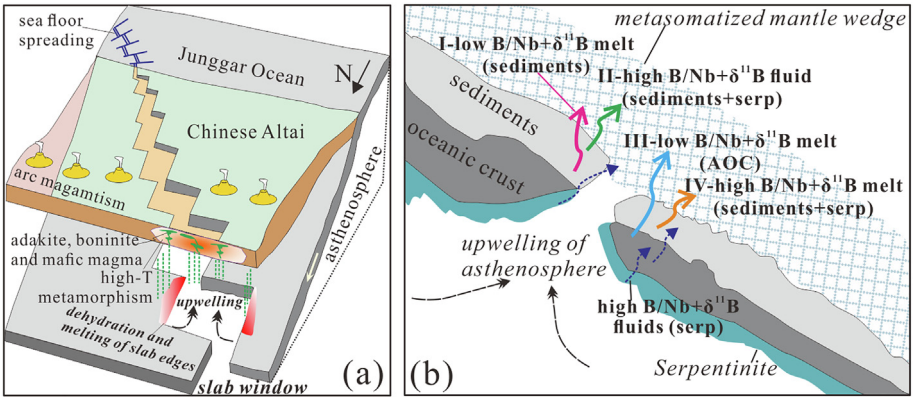

Fig. 7. Cartoons show (a) upwelling of the asthenosphere mantle through the slab window during the middle Paleozoic ridge subduction in the Chinese Altai, which caused intense dehydration and melting of the subducted slab along edges (modified after Windley and Xiao (2018)); (b) fluids and melts from the subducted sediments, oceanic crust and serpentinite have variable B contents and isotopic compositions, and transferred different amount of water into the mantle wedge.

Zr/Yb and Nb/Yb (Fig. 6), denoting that melting degrees of their mantle sources increase with elevation of water flux.

5.4. Intense dehydration and melting of subducted slab due to ridge subduction

The Chinese Altai possibly underwent the oceanic ridge subduction in the middle Paleozoic (Fig. 7) with peak times of 400–390 Ma (Sun et al., 2009) and 382–360 Ma (Cai et al., 2010; Windley and Xiao, 2018; Yu et al., 2020), which have been documented by the occurrences of adakites and high-Ca boninites (Niu et al., 2006; Windley and Xiao, 2018) and intensive melting of the subducted slab (Yu et al., 2017a, 2020). The Habahe mafic dikes emplaced at ~360 Ma show variable geochemical and Sr-Nd-Pb-B isotopic compositions, denoting the intense dehydration

and melting of the subducted slab within a short distance during ridge subduction (Fig. 7; Yu et al., 2020). Melting of subducted slab is a typical process during ridge subduction (DeLong et al., 1978; Johnston and Thorkelson, 1997) because the subducted slab near the oceanic ridge is young and hot (DeLong et al., 1978; Defant and Drummond, 1990). Furthermore, a slab window would be formed during ridge subduction, due to progressive unzipping of the oceanic ridge, which can facilitate ascending of the hot sub-slab asthenospheric mantle (Thorkelson and Breitsprecher, 2005). Upwelling of asthenospheric mantle will cause sharp increase of surface temperature for the subducted slab and induce intense slab dehydration and melting (Fig. 7a; DeLong et al., 1978; Johnston and Thorkelson, 1997; Thorkelson and Breitsprecher, 2005). Thus, coeval magmatism in and around the slab window are geochemically different due to distinct temperatures, such as adakitic/boninitic melts derived from the slab edges and other more typical arc magmatism away from the slab window (Niu et al., 2006; Windley and Xiao, 2018). On the other hand, various subduction components from subducted oceanic crust, sediments and serpentinite near the slab window might transfer different amount of water into the mantle sources, which can account for variable geochemical and Sr-Nd-Pb-B isotopic compositions of the Habahe mafic dikes within short distance (Fig. 7b).

5.5. Role of water flux on melting in the mantle wedge in global subduction zone

It is widely agreed that the influx of water from subducted slab can lower the solidus of peridotite and then enhance melting degree of the mantle wedge (Fig. 8; Gaetani and Grove, 1998; Kelley et al., 2010; Till et al., 2012; Green, 2015; Mallik et al., 2015). On the other hand, the extent of melting of the mantle wedge in arcs might also be controlled by the thickness of the overlying plate (Turner and Langmuir, 2015a, b; Turner et al., 2016) and tends to decrease with increasing thickness of the overlying lithosphere. To further investigate the role of H_2O flux and crustal thickness in melting of the mantle wedge, we compared the Habahe mafic dikes with IABs from the Cascade, Central America and Tonga-Kermadec-New Zealand (TKNZ) arcs (Leeman et al., 2004; 2017; Tonarini et al., 2007).

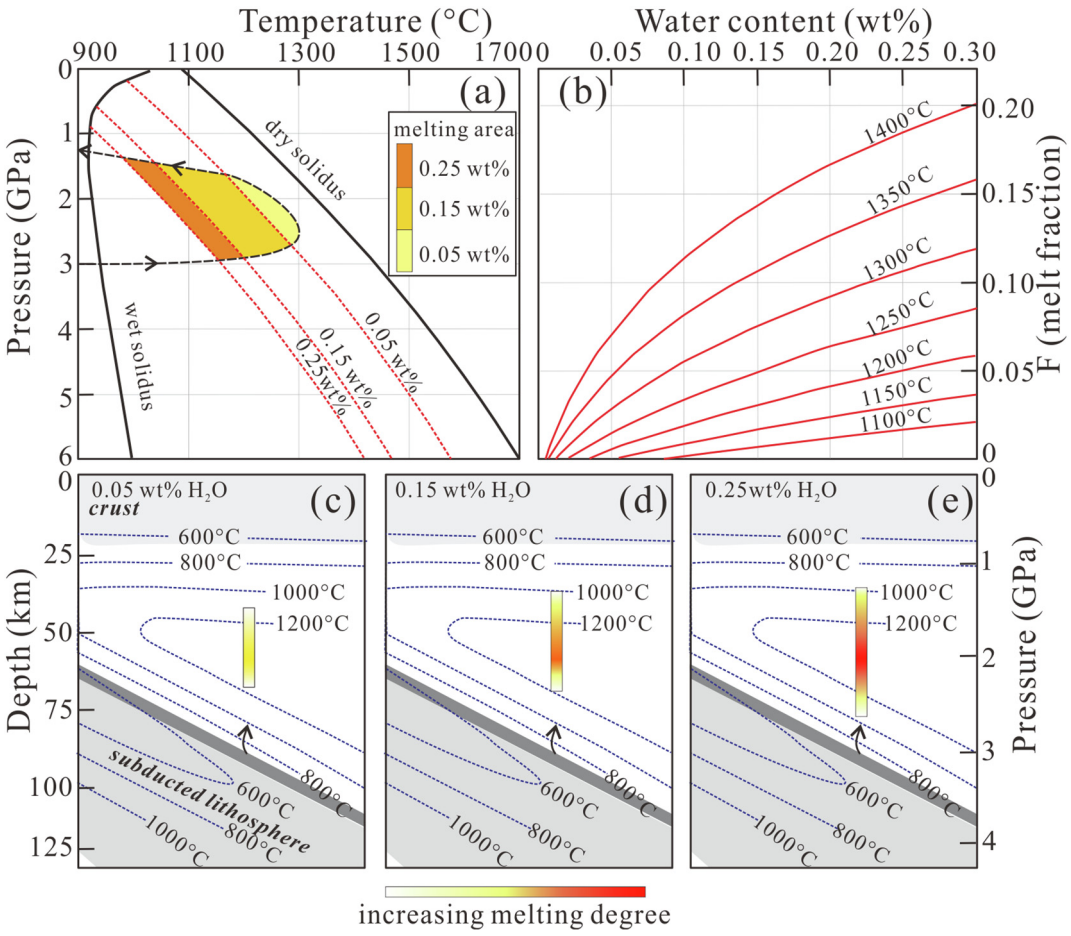

Fig. 8. (a) Solidus and melting area of the mantle peridotite with addition of variable amount of water; (b) variation of melt fraction (F) with different amount of water in mantle peridotite; (c–e) variation of melting area and extent in the mantle wedge with different amount of water (0.05–0.25 wt%). The solidus of peridotite in (a) and melt fraction in (b) with different amount of water are calculated based on Kelley et al. (2010).

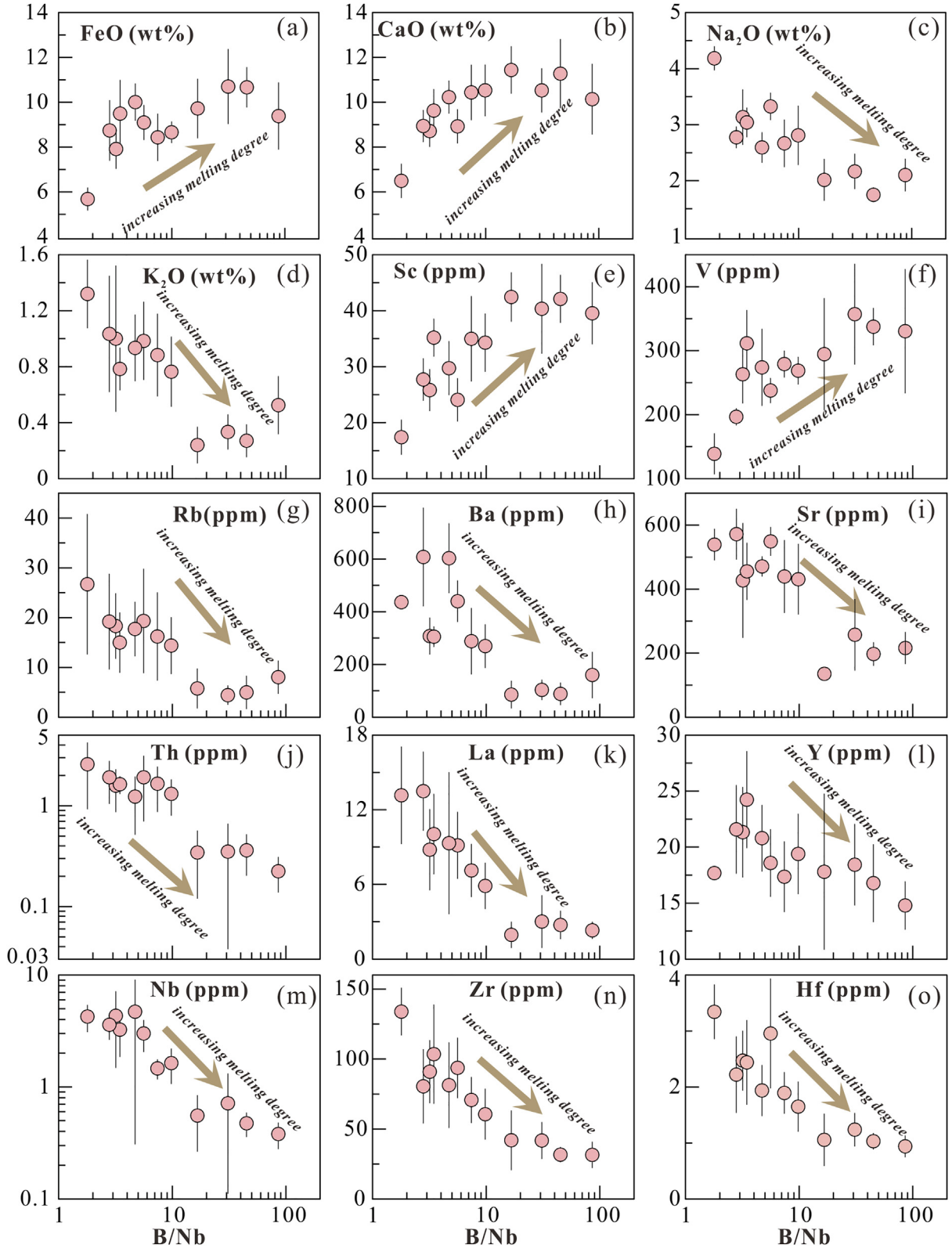

Fig. 9. Bivariate diagrams of B/Nb and major and trace elements for IABs from the global arcs, with data compiled from Turner and Langmuir (2015a).

The Cascade and Central America arcs are all typical hot subduction zones and have a crustal thickness of ~40 km and ~45 km, respectively (Syracuse et al., 2010), which could be slightly thicker than the middle Paleozoic crust in the Chinese Altai (30–35 km; Jiang et al., 2016). The Habahe Type-I and -III mafic dikes and IABs from the Central America arcs show similar Zr/Yb and Nb/Yb, which are much lower than IABs from the Cascade arc (Fig. 6). This denotes that they were formed through higher degree melting of the mantle wedge than that of the Cascade IABs. Thus, different extents of melting of the mantle wedge in these arcs cannot be explained by variations in crustal thickness. On the other hand, IABs from the Cascade arc show low B/Nb and negative $\delta^{11}B$ values, indicating low input of H_2O into their mantle source (Leeman et al., 2004). This is because the subducting slab beneath the Cascade arc has high surface temperature (Syracuse et al. 2010) and most of the water inventory (~98%) has escaped from the slab before arriving at the sub-arc depths (~100 km; Leeman et al., 2004; van Keken et al., 2011). The subducting slab in the Central America arc also has high surface temperature similar to the Cascade arc and may also have undergone significant loss of water at shallow subduction depth (Syracuse et al. 2010; van Keken et al., 2011). However, IABs from the Central America arc mostly show positive $\delta^{11}B$ values similar to Type-IV mafic dikes in this study (Fig. 6c, d), which is interpreted as involvement of fluids from the slab serpentinite in their mantle source (Tonarini et al., 2007). Dehydration of the slab serpentinite can supply high amount of water to the mantle wedge to enhance its melting extent, which is responsible for higher B/Nb and lower Zr/Yb and Nb/Yb ratios in IABs from the Central America arc than those from the Cascade arc. In contrast, the subducted slab segments in the TKNZ arcs are cold and can carry more water to the sub-arc depth (Syracuse et al. 2010; van Keken et al., 2011). Thus, IABs from the TKNZ arcs (Leeman et al., 2017) show much higher B/Nb ratios than those from the Central America and Cascade arcs (Fig. 6), indicating higher water flux beneath the TKNZ arcs. This may cause larger degree melting of the mantle wedge in the TKNZ arcs, which is evidenced by lower Zr/Yb and Nb/Yb in IABs from the TKNZ than those from the Central America and Cascade arcs (Fig. 6). Similarly, Type-II and Type-IV mafic dikes in the Habahe area have higher B/Nb and lower Zr/Yb and Nb/Yb ratios than Type-I and Type-III mafic dikes (Fig. 6), due to relatively higher water flux in their mantle sources. As a whole, the Habahe mafic dikes and IABs from the Cascade, Central America and TKNZ arcs show negative correlations between B/Nb and Zr/Yb, and B/Nb and Nb/Yb (Fig. 6), denoting that the varying melting degrees of the mantle wedge peridotite were mainly caused by different water flux in these arcs.

Furthermore, IABs from global arcs show wide range of B/Nb ratios, which are also well correlated with Zr/Yb and Nb/Yb ratios (Fig. 6). This demonstrates that the mantle wedge in global arcs undergoes different extents of melting due to the difference in water flux. More importantly, major and trace elements of IABs from the global arcs exhibit robust correlations with B/Nb (Fig. 9), indicating that H_2O should have strongly controlled the partial melting of mantle wedge and IAB compositions.

6. CONCLUDING SUMMARY

The mantle sources of the Habahe mafic dikes were metasomatized by different components from the subducted sediments, oceanic crust and serpentinite. Melts from the subducted sediments and oceanic crust have lighter B isotopic compositions and lower B/Nb than fluids from the slab serpentinite. Dehydration of the slab serpentinite transferred more H_2O into the mantle sources of the Habahe mafic dikes and cause higher degree melting of the mantle wedge. Wide range of B/Nb ratios also appear for global IABs, which reflects variation of water input into the mantle wedge. This study provokes that the water flux plays an important role on melting in the mantle wedge and controls IAB compositions in global arcs.

Declaration of Competing Interest

The authors declare that they have no known competing financial interests or personal relationships that could have appeared to influence the work reported in this paper.

ACKNOWLEDGEMENTS

We thank L. Zhang and X.L. Tu for analytical assistance. We would also like to thank the careful and thoughtful comments of R. Halama, W. P. Leeman, and four anonymous reviewers, which strongly improved the manuscript. This study was financially supported by the National Natural Science Foundation of China (NSFC Projects 41890812, 41902056, 41625007), China Postdoctoral Science Foundation (2018M633172) and the Key Special Project for Introduced Talents Team of Southern Marine Science and Engineering Guangdong Laboratory (Guangzhou) (GML2019ZD0202). This is contribution No. IS-3010 from GIG-CAS.

APPENDIX A. SUPPLEMENTARY DATA

Supplementary data to this article can be found online at https://doi.org/10.1016/j.gca.2021.03.032.

REFERENCES

Adam J. and Green T. (2006) Trace element partitioning between mica- and amphibole-bearing garnet lherzolite and hydrous basanitic melt: 1. Experimental results and the investigation of controls on partitioning behavior. *Contrib. Mineral. Petrol.* **152** (1), 1–17.

Bebout G. E. and Nakamura E. (2003) Record in metamorphic tourmalines of subduction-zone devolatilization and boron cycling. *Geology* **31**, 407–410.

Brenan J. M., Ryerson F. J. and Shaw H. R. (1998) The role of aqueous fluids in the slab-to-mantle transfer of boron, beryllium, and lithium during subduction: Experiments and model. *Geochim. Cosmochim. Acta* **62**, 3337–3347.

Cai K. D., Sun M., Yuan C., Zhao G. C., Xiao W. J., Long X. P. and Wu F. Y. (2010) Geochronological and geochemical study of mafic dykes from the northwest Chinese Altai: Implications

for petrogenesis and tectonic evolution. *Gondwana Res.* **18**, 638–652.

Cai K. D., Sun M., Yuan C., Zhao G. C., Xiao W. J., Long X. P. and Wu F. Y. (2011) Prolonged magmatism, juvenile nature and tectonic evolution of the Chinese Altai, NW China: Evidence from zircon U-Pb and Hf isotopic study of Paleozoic granitoids. *J. Asian Earth Sci.* **42**, 949–968.

Carmichael I. S. E. (2002) The andesite aqueduct: perspectives on the evolution of intermediate magmatism in west-central (105–99°W) Mexico. *Contrib. Mineral. Petrol.* **143**, 641–663.

Catlos E. J. and Sorensen S. S. (2003) Phengite-based chronology of K- and Ba-rich fluid flow in two paleosubduction zones. *Science* **299**(5603), 92–95.

Chen B. and Jahn B. M. (2002) Geochemical and isotopic studies of the sedimentary and granitic rocks of the Altai orogen of northwest China and their tectonic implications. *Geolog. Mag.* **139**, 1–13.

Cooper G. F., Macpherson C. G., Blundy J. D., Maunder B., Allen R. W., Goes S., Collier J. S., Bie L. D., Harmon N., Hicks S. P., Iveson A. A., Prytulak J., Rietbrock A., Rychert C. A. and Davidson J. P. (2020) Variable water input controls evolution of the Lesser Antilles volcanic arc. *Nature* **582**, 525–529.

Defant M. J. and Drummond M. S. (1990) Derivation of some modern arc magmas by melting of young subducted lithosphere. *Nature* **347**, 662–665.

De Hoog C. J. and Savov I. P. (2018) Boron Isotopes as a Tracer of Subduction Zone Processes. In: Boron Isotopes-The Fifth Element. In: Advances in Isotope Geochemistry 9, 217–247.

DeLong S. E., Fox P. J. and McDowell F. W. (1978) Subduction of the Kula ridge at the Aleutian trench. *Geol. Soc. Am. Bull.* **89**, 83–95.

Deschamps F., Godard M., Guillot S. and Hattori K. (2013) Geochemistry of subduction zone serpentinites: A review. *Lithos* **178**, 96–127.

Elkins L., Gaetani G. and Sims K. (2008) Partitioning of U and Th during garnet pyroxenite partial melting: Constraints on the source of alkaline ocean island basalts. *Earth Planet Sci. Lett.* **265**, 270–286.

Elliott T., Plank T., Zindler A., White W. and Bourdon B. (1997) Element transport from slab to volcanic front at the Mariana Arc. *J. Geophys. Res.* **102**(7), 14991–15019.

England P. C. and Katz R. F. (2010) Melting above the anhydrous solidus controls the location of volcanic arcs. *Nature* **467**(7316), 700–703.

Foster G. L., Pogge von Strandmann P. A. E. and Rae J. W. B. (2010) Boron and magnesium isotopic composition of seawater. *Geochem. Geophys. Geosyst.* **11**(Q08), 015.

Gaetani G. A. and Grove T. L. (1998) The influence of water on melting of mantle peridotite. *Contrib. Mineral. Petrol.* **131**, 323–346.

Gaillardet, J., Lemarchand, D. (2018). Boron in the Weathering Environment. In: Boron Isotopes-The Fifth Element. In: Advances in Isotope Geochemistry 9, 163–188.

Green D. H. (2015) Experimental petrology of peridotites, including effects of water and carbon on melting in the Earth's upper mantle. *Phys. Chem. Miner.* **42**, 95–122.

Grove T. L., Parman S. W., Bowring S. A., Price R. C. and Baker M. B. (2002) The role of an H_2O-rich fluid component in the generation of primitive basaltic andesites and andesites from the Mt. Shasta region, N California. *Contrib. Mineral. Petrol.* **142**(4), 375–396.

Grove T. L., Chatterjee N., Parman S. W. and Medard E. (2006) The influence of H_2O on mantle wedge melting. *Earth Planet. Sci. Lett.* **249**, 74–89.

Grove T. L., Till C. B., Lev E., Chatterjee N. and Medard E. (2009) Kinematic variables and water transport control the formation and location of arc volcanoes. *Nature* **459**, 694–697.

Grove T. L., Till C. B. and Krawczynski M. J. (2012) The role of H_2O in subduction zone magmatism. *Ann. Rev. Earth Planet. Sci.* **40**, 413–439.

Hermann J. and Rubatto D. (2009) Accessory phase control on the trace element signature of sediment melts in subduction zones. *Chem. Geol.* **265**, 512–526.

Hervig R. L., Moore G. M., Williams L. B., Peacock S. M., Holloway J. R. and Roggensack K. (2002) Isotopic and elemental partitioning of boron between hydrous fluid and silicate melt. *Am. Mineral.* **87**(5–6), 769–774.

Hyndman R. D. and Peacock S. M. (2003) Serpentinization of the forearc mantle. *Earth Planet. Sci. Lett.* **212**(3–4), 417–432.

Ishikawa T. and Nakamura E. (1993) Boron isotope systematics of marine sediments. *Earth Planet. Sci. Lett.* **117**, 567–580.

Ishikawa T. and Tera F. (1999) Two isotopically distinct fluid components involved in the Mariana arc: evidence from Nb/B ratios and B, Sr, Nd, and Pb isotope systematics. *Geology* **27**(1), 83–86.

Ishikawa T., Tera F. and Nakazawa T. (2001) Boron isotope and trace element systematics of the three volcanic zones in the Kamchatka arc. *Geochim. Cosmochim. Acta* **65**, 4523–4537.

Jiang Y. D., Sun M., Zhao G. C., Yuan C., Xiao W. J., Xiao X. P., Long X. P. and Wu F. Y. (2010) The 390 Ma high-T metamorphism in the Chinese Altai: consequence of ridge subduction? *Am. J. Sci.* **310**, 1421–1452.

Jiang Y. D., Schulmann K., Sun M., Stipska P., Guy A., Janousek V., Lexa O. and Yuan C. (2016) Anatexis of accretionary wedge, Pacific-type magmatism, and formation of vertically stratified continental crust in the Altai Orogenic Belt. *Tectonics.* **35**(12), 3095–3118.

Jochum K. P., Weis U., Schwager B., Stoll B., Wilson S. A., Haug G. H., Andreae M. O. and Enzweiler J. (2016) Reference Values Following ISO Guidelines for Frequently Requested Rock Reference Materials. *Geostand. Geoanal. Res.* **40**(3), 333–350.

Johnston S. T. and Thorkelson D. J. (1997) Cocos-Nazca slab window beneath Central America. *Earth Planet. Sci. Lett.* **146**, 465–474.

Kawamoto T. and Holloway J. R. (1997) Melting temperature and partial melt chemistry of H_2O-saturated mantle peridotite to 11 gigapascals. *Science* **276**(5310), 240–243.

Kelley K. A., Plank T., Grove T. L., Stolper E. M., Newman S. and Hauri E. H. (2006) Mantle melting as a function of water content beneath back-arc basins. *J. Geophys. Res.* **111**, B09208.

Kelley K. A., Plank T., Newman S., Stolper E. M., Grove T. L., Parman S. and Hauri E. H. (2010) Mantle melting as a function of water content beneath the Mariana Arc. *J. Petrol.* **51**(8), 1711–1738.

Kessel R., Schmidt M. W., Ulmer P. and Pettke T. (2005) Trace element signature of subduction-zone fluids, melts and supercritical liquids at 120–180 km depth. *Nature* **437**, 724–727.

Klimm K., Blundy J. D. and Green T. H. (2008) Trace element partitioning and accessory phase saturation during H_2O-saturated melting of basalt with implications for subduction zone chemical fluxes. *J. Petrol.* **49**, 523–553.

Konrad-Schmolke M. and Halama R. (2014) Combined thermodynamic-geochemical modeling in metamorphic geology: boron as tracer of fluid-rock interaction. *Lithos* **208**, 393–414.

Konrad-Schmolke M., Halama R. and Manea V. C. (2016) Slab mantle dehydrates beneath Kamchatka-yet recycles water into the deep mantle. *Geochem. Geophys. Geosyst.* **17**(8), 2987–3007.

Kowalski P. M., Wunder B. and Jahn S. (2013) Ab initio prediction of equilibrium boron isotope fractionation between minerals

and aqueous fluids at high P and T. *Geochim Cosmochim Acta* **101**, 285–301.

Kowalski P. M. and Wunder B. (2018) Boron Isotope Fractionation Among Vapor-Liquids-Solids-Melts: Experiments and Atomistic Modeling. In: Boron Isotopes-The Fifth Element. In: Advances in Isotope Geochemistry 3, 33–69.

Leeman W. P. (1996) Boron and other fluid-mobile elements in volcanic arc lavas: Implications for subduction processes. *Subduction Top to Bottom, AGU Monograph* **96**, 269–276.

Leeman W. P., Tonarini S., Chan L. H. and Borg L. M. (2004) Boron and lithium isotopic variations in a hot subduction zone-The southern Washington Cascades. *Chem. Geol.* **212**, 101–124.

Leeman W. P., Tonarini S. and Turner S. (2017) Boron isotope variations in Tonga-Kermadec-New Zealand arc lavas: implications for origin of subduction components and mantle influences. *Geochem. Geophys. Geosyst.* **18**, 1126–1162.

Li X., Li H. Y., Ryan J. G., Wei G. J., Zhang L., Li N. B., Huang X. L. and Xu Y. G. (2019) High-precision measurement of B isotopes on low-boron oceanic volcanic rock samples via MC-ICPMS: Evaluating acid leaching effects on boron isotope compositions, and B isotopic variability in depleted oceanic basalts. *Chem. Geol.* **505**, 76–85.

Lundstrom C. C., Shaw H. F., Ryerson F. J., Williams Q. and Gill J. (1998) Crystal chemical control of clinopyroxene-melt partitioning in the Di-Ab-An system: Implications for elemental fractionations in the depleted mantle. *Geochim. Cosmochim. Acta* **62**(16), 2849–2862.

Mallik A., Nelson J. and Dasgupta R. (2015) Partial melting of fertile peridotite fluxed by hydrous rhyolitic melt at 2–3 GPa: implications for mantle wedge hybridization by sediment melt and generation of ultrapotassic magmas in convergent margins. *Contrib. Mineral. Petrol.* **169**, 48.

Manea V. C., Leeman W. P., Gerya T., Manea M. and Zhu G. (2014) Subduction of fracture zones controls mantle melting and geochemical signature above slabs. *Nat. Commun.* **5**, 5095.

Maner J. L. and London D. (2018) Fractionation of the isotopes of boron between granitic melt and aqueous solution at 700 ℃ and 800 ℃ (200 MPa). *Chem. Geol.* **489**, 16–27.

Marschall H. R., Altherr R. and Rüpke L. (2007) Squeezing out the slab-modelling the release of Li, Be and B during progressive high-pressure metamorphism. *Chem. Geol.* **239**(3–4), 323–335.

Marschall H. R., Altherr R., Kalt A. and Ludwig T. (2008) Detrital, metamorphic and metasomatic tourmaline in high-pressure metasediments from Syros (Greece): intra-grain boron isotope patterns determined by secondary-ion mass spectrometry. *Contrib. Mineral. Petrol.* **155**(6), 703–717.

Marschall H. R., Wanless V. D., Shimizu N., von Strandmann P. A. P., Elliott T. and Monteleone B. D. (2017) The boron and lithium isotopic composition of mid-ocean ridge basalts and the mantle. *Geochim. Cosmochim. Acta* **207**, 102–138.

Martin C., Flores K. E. and Harlow G. E. (2016) Boron isotopic discrimination for subduction related serpentinites. *Geology* **44** (11), 899–902.

Martin C., Flores K. E., Vitale-Brovarone A., Angiboust S. and Harlow G. E. (2020) Deep mantle serpentinization in subduction zones: Insight from in situ B isotopes in slab and mantle wedge serpentinites. *Chem. Geol.* **545** 119637.

Mysen B. O. and Boettcher A. L. (1975) Melting of a hydrous mantle 1. Phase relations of natural peridotite at high-pressures and temperatures with controlled activities of water, carbon-dioxide, and hydrogen. *J. Petrol.* **16**(3), 520–548.

Nakano T. and Nakamura E. (2001) Boron isotope geochemistry of metasedimentary rocks and tourmalines in a subduction zone metamorphic suite. *Phys. Earth Planet. Inter.* **127**, 233–252.

Niu H. C., Hiroaki S., Zhang H. X., Jun'ichi I., Yu X. Y., Nagao T., Terada K. and Zhang Q. (2006) Juxtaposition of adakite, boninite, high-TiO_2 and low-TiO_2 basalts in the Devonian southern Altay, Xinjiang, NW China. *J. Asian Earth Sci.* **28**, 439–456.

Pabst S., Zack T., Savov I. P., Ludwig T. and Rost D. (2012) The fate of subducted oceanic slabs in the shallow mantle: Insights from boron isotopes and light elemnt composition of metasomatized blueschists from the Mariana forearc. *Lithos* **132–133**, 162–179.

Perrin A., Goes S., Prytulak J., Rondenay S. and Davies D. R. (2018) Mantle wedge temperatures and their potential relation to volcanic arc location. *Earth Planet. Sci. Lett.* **501**, 67–77.

Pichavant M. and MacDonald R. (2007) Crystallization of primitive basaltic magmas at crustal pressures and genesis of the calcalkaline igneous suite: experimental evidence from St Vincent, Lesser Antilles arc. *Contrib. Mineral. Petrol.* **154**(5), 535–558.

Plank T. and Langmuir C. H. (1998) The chemical composition of subducting sediment: implications for the crust and mantle. *Chem. Geol.* **145**, 325–394.

Plank T., Kelley K. A., Zimmer M. M., Hauri E. H. and Wallace P. J. (2013) Why do mafic magmas contain ~4 wt% water on average? *Earth Planet Sci. Lett.* **364**, 168–179.

Pouchou J. L. and Pichoir F. (1991). Quantitative Analysis of Homogeneous or Stratified Microvolumes Applying the Model "PAP". In Electron Probe Quantification, (eds. K. F. J. Heinrich and D. E. Newbury), 31–75.

Rosner M. and Meixner A. (2004) Boron isotopic composition and concentration of ten geological reference materials. *Geostand. Geoanal. Res.* **28**(3), 431–441.

Rüpke L. H., Morgan J. P., Hort M. and Connolly J. A. D. (2004) Serpentine and the subduction zone water cycle. *Earth Planet. Sci. Lett.* **223**(1–2), 17–34.

Ryan J. G. and Chauvel C. (2014) The Subduction-Zone Filter and the Impact of Recycled Materials on the Evolution of the Mantle. In Treatise on Geochemistry (Second Edition, eds. H. D. Holland and K. K. Turekian), 479–508.

Salters V. J. M. and Stracke A. (2004) Composition of the depleted mantle. *Geochem. Geophys. Geosyst.* **5**(5).

Salters V. J. M. and Longhi J. (1999) Trace element partitioning during the initial stages of melting beneath mid-ocean ridges. *Earth Planet. Sci. Lett.* **166**, 15–30.

Savov I. P., Ryan J. G., D'Antonio M. and Fryer P. (2007) Shallow slab fluid release across and along the Mariana arc-basin system: insights from geochemistry of serpentinized peridotites from the Mariana fore arc. *J. Geophys. Res.* **112**(B9), B09205.

Scambelluri M., Müntener O., Ottolini L., Pettke T. T. and Vannucci R. (2004) The fate of B, Cl and Li in the subducted oceanic mantle and in the antigorite breakdown fluids. *Earth Planet. Sci. Lett.* **222**, 217–234.

Scambelluri M. and Tonarini S. (2012) Boron isotope evidence for shallow fluid transfer across subduction zones by serpentinized mantle. *Geology* **40**, 907–910.

Shaw D. M. (2000) Continuous (dynamic) melting theory revisited. *Can. Mineral.* **38**, 1041–1063.

Sisson T. W. and Grove T. L. (1993) Experimental investigations of the role of H_2O in Calc-Alkaline differentiation and subduction zone magmatism. *Contrib. Mineral. Petrol.* **113**(2), 143–166.

Spandler C. and Pirard C. (2013) Element recycling from subducting slabs to arc crust: A review. *Lithos* **170**, 208–223.

Spivack A. J., Palmer M. R. and Edmond J. M. (1987) The sedimentary cycle of the boron isotopes. *Geochim. Cosmochim. Acta* **51**(7), 1939–1949.

Spivack A. J. and Edmond J. M. (1987) Boron isotope exchange between seawater and the oceanic crust. *Geochim. Cosmochim. Acta* **51**, 1033–1043.

Sugden P. J., Savov I. P., Agostini S., Wilson M., Halama R. and Meliksetian K. (2020) Boron isotope insights into the origin of subduction signatures in continent-continent collision zone volcanism. *Earth Planet. Sci. Lett.* **538** 116207.

Sun M., Yuan C., Xiao W. J., Long X. P., Xia X. P., Zhao G. C., Lin S. F., Wu F. Y. and Kroner A. (2008) Zircon U-Pb and Hf isotopic study of gneissic rocks from the Chinese Altai: Progressive accretionary history in the early to middle Palaeozoic. *Chem. Geol.* **247**, 352–383.

Sun M., Long X. P., Cai K. D., Jiang Y. D., Wang B., Yuan C., Zhao G. C., Xiao W. J. and Wu F. Y. (2009) Early Paleozoic ridge subduction in the Chinese Altai: Insight from the abrupt change in zircon Hf isotopic compositions. *Sci. China Ser. D* **52**, 1345–1358.

Sun S. S. and McDonough W. F. (1989) Chemical and isotopic systematics of oceanic basalts: implication for mantle composition and process. In Magmatism in the ocean Basins. (eds. A. D. Sauders, M.J. Norry). Geolog. Soc. Lond. Spec. Publ. 42, 313–345.

Syracuse E. M., van Keken P. E. and Abers G. A. (2010) The global range of subduction zone thermal models. *Phys. Earth Planet. Inter.* **183**, 73–90.

Thompson G. and Melson W. G. (1970) Boron contents of serpentinites and metabasalts in the oceanic crust: implicatons for the boron cycle in the oceans. *Earth Planet. Sci. Lett.* **8**, 61–65.

Thorkelson D. J. and Breitsprecher K. (2005) Partial melting of slab window margins: genesis of adakitic and non-adakitic magmas. *Lithos* **79**, 25–41.

Till C. B., Grove T. L. and Withers A. C. (2012) The beginnings of hydrous mantle wedge melting. *Contrib. Mineral. Petrol.* **163**, 669–688.

Tonarini S., Pennisi M., Adorni-Braccesi A., Dini A., Ferrara G., Gonfiantini R., Wiedenbeck M. and Gröning M. (2003) Intercomparison of boron isotope and concentration measurements. Part I, selection, preparation and homogeneity tests of the intercomparison materials. *Geostand. Geoanal. Res.* **27**(1), 21–39.

Tonarini S., Agostini S., Doglioni C., Innocenti F. and Manetti P. (2007) Evidence for serpentinite fluid in convergent margin systems: The example of El Salvador (Central America) arc lavas. *Geochem. Geophys. Geosyst.* **8**, Q09014.

Trumbull R. B. and Slack J. F. (2018) Boron Isotopes in the Continental Crust: Granites, Pegmatites, Felsic Volcanic Rocks, and Related Ore Deposits. In: Boron Isotopes-The Fifth Element. In: Advances in Isotope Geochemistry 10, 249–272.

Turner S. J. and Langmuir C. H. (2015a) The global chemical systematics of arc front stratovolcanoes: Evaluating the role of crustal processes. *Earth Planet. Sci. Lett.* **422**, 182–193.

Turner S. J. and Langmuir C. H. (2015b) What processes control the chemical compositions of arc front stratovolcanoes? *Geochem. Geophys. Geosyst.* **16**, 1865–1893.

Turner S. J., Langmuir C. H., Katz R. F., Dungan M. A. and Escrig S. (2016) Parental arc magma compositions dominantly controlled by mantle-wedge thermal structure. *Nat. Geosci.* **9**, 772–776.

van Keken P. E., Hacker B. R., Syracuse E. M. and Abers G. A. (2011) Subduction factory: 4. Depth-dependent flux of H_2O from subducting slabs worldwide. *J. Geophys. Res.* **116**, B01401.

Wada I. and Wang K. (2009) Common depth of slab-mantle decoupling: Reconciling diversity and uniformity of subduction zones. *Geochem. Geophys. Geosyst.* **10**(10), Q10009.

Wei G. J., Wei J. X., Liu Y., Ke T., Ren Z. Y., Ma J. L. and Xu Y. G. (2013) Measurement on high-precision boron isotope of silicate materials by a single column purification method and MC-ICP-MS. *J. Anal. At. Spectrom.* **28**(4), 606–612.

Windley B. F., Alexeiev D., Xiao W. J., Kröner A. and Badarch G. (2007) Tectonic models for accretion of the Central Asian Orogenic Belt. *J. Geolog. Soc.* **164**, 31–47.

Windley B. F. and Xiao W. J. (2018) Ridge subduction and slab windows in the Central Asian Orogenic Belt: Tectonic implications for the evolution of an accretionary orogen. *Gondwana Res.* **61**, 73–87.

Wu J. and Stebbins J. F. (2010) Quench rate and temperature effects on boron coordination in aluminoborosilicates. *J. Non-Cryst. Solids* **356**, 2097–2108.

Wunder B., Meixner A., Romer R. L., Wirth R. and Heinrich W. (2005) The geochemical cycle of boron: constraints from boron isotope partitioning experiments between mica and fluid. *Lithos* **84**, 206–216.

Xiao W. J., Windley B., Sun S., Li J. L., Huang B. C., Han C. M., Yuan C., Sun M. and Chen H. L. (2015) A Tale of Amalgamation of Three Permo-Triassic Collage Systems in Central Asia: Oroclines, Sutures, and Terminal Accretion. *Ann. Rev. Earth Planet. Sci.* **43**, 407–507.

Xu R., Romer R. and Glodny J. (2021) External fluids cause alteration and metal redistribution in the granite-hosted Tangziwa Sn-Cu deposit, Gejiu district, China. *Lithos* **382–383** 105937.

Yamada C., Tatsuki T., Chang Q. and Kimura J. (2019) Boron isotope variations of Franciscan serpentinites, northern California. *Lithos* **334–335**, 180–189.

You C. F., Chan L. H., Spivack A. J. and Gieskes J. M. (1995) Lithium, boron, and their isotopes in sediments and pore waters of Ocean drilling program site-808, Nankai trough-implications for fluid expulsion in accretionary prisms. *Geology* **23**(1), 37–40.

You C. F., Spivack A. J., Gieskes J. M., Martin J. B. and Davisson M. L. (1996) Boron contents and isotopic compositions in pore waters: a new approach to determine temperature induced artifacts-geochemical implications. *Mar. Geol.* **129**(3–4), 351–361.

Yu Y., Sun M., Huang X. L., Zhao G. C., Li P. F., Long X. P., Cai K. D. and Xia X. P. (2017a) Sr-Nd-Hf-Pb isotopic evidence for modification of the Devonian lithospheric mantle beneath the Chinese Altai. *Lithos* **284–285**, 207–221.

Yu Y., Sun M., Long X. P., Li P. F., Zhao G. C., Kröner A., Broussolle A. and Yang J. H. (2017b) Whole-rock Nd-Hf isotopic study of I-type and peraluminous granitic rocks from the Chinese Altai: Constraints on the nature of the lower crust and tectonic setting. *Gondwana Res.* **47**, 131–141.

Yu Y., Sun M., Yuan C., Zhao G. C., Huang X. L., Rojas-Agramonte Y. and Chen Q. (2019) Evolution of the middle Paleozoic magmatism in the Chinese Altai: constraints on the crustal differentiation at shallow depth in the accretionary orogen. *J. Asian Earth Sci.* **175**, 230–246.

Yu Y., Huang X. L., Sun M. and Yuan C. (2020) Missing Sr-Nd isotopic decoupling in subduction zone: Decoding the multi-stage dehydration and melting of subducted slab in the Chinese Altai. *Lithos* **362–363** 105465.

Associate editor: Ralf Halama